frontiers in Marine Science

ORIGINAL RESEARCH
published: 22 March 2021
doi: 10.3389/fmars.2021.632087

Low Fe Availability for Photosynthesis of Sea-Ice Algae: *Ex situ* Incubation of the Ice Diatom *Fragilariopsis cylindrus* in Low-Fe Sea Ice Using an Ice Tank

Kazuhiro Yoshida[1,2†], Andreas Seger[2], Matthew Corkill[2,3], Petra Heil[3,4,5], Kristen Karsh[3], Andrew McMinn[2,3*] and Koji Suzuki[1,6*]*

[1] Graduate School of Environmental Science, Hokkaido University, Sapporo, Japan, [2] Institute for Marine and Antarctic Studies, University of Tasmania, Battery Point, TAS, Australia, [3] Antarctic Climate and Ecosystems Cooperative Research Centre, University of Tasmania, Battery Point, TAS, Australia, [4] Australian Antarctic Programme Partnership, University of Tasmania, Battery Point, TAS, Australia, [5] Australian Antarctic Division, Kingston, TAS, Australia, [6] Faculty of Environmental Earth Science, Hokkaido University, Sapporo, Japan

Sea-ice algae play a crucial role in the ecology and biogeochemistry of sea-ice zones. They not only comprise the base of sea-ice ecosystems, but also seed populations of extensive ice-edge blooms during ice melt. Ice algae must rapidly acclimate to dynamic light environments, from the low light under sea ice to high light within open waters. Recently, iron (Fe) deficiency has been reported for diatoms in eastern Antarctic pack ice. Low Fe availability reduces photosynthetic plasticity, leading to reduced ice-algal primary production. We developed a low-Fe ice tank to manipulate Fe availability in sea ice. Over 20 days in the ice tank, the Antarctic ice diatom *Fragilariopsis cylindrus* was incubated in artificial low-Fe sea ice ([total Fe] = 20 nM) in high light (HL) and low light (LL) conditions. Melted ice was also exposed to intense light to simulate light conditions typical for melting ice *in situ*. When diatoms were frozen in, the maximum photochemical quantum efficiency of photosystem II (PSII), F_v/F_m, was suppressed by freezing stress. However, the diatoms maintained photosynthetic capability throughout the ice periods with a stable F_v/F_m value and increased photoprotection through non-photochemical quenching (NPQ) via photoprotective xanthophyll cycling (XC) and increased photoprotective carotenoid levels compared to pre-freeze-up. Photoprotection was more pronounced in the HL treatment due to greater light stress. However, the functional absorption cross section of PSII, σ_{PSII}, in *F. cylindrus* consistently increased after freezing, especially in the LL treatment ($\sigma_{PSII} > 10$ nm^2 PSII^{-1}). Our study is the first to report such a large σ_{PSII} in ice diatoms at low Fe conditions. When the melted sea ice was exposed to high light, F_v/F_m was suppressed. NPQ and XC were slightly upregulated, but not to values normally observed when Fe is not limiting, which indicates reduced photosynthetic flexibility to

OPEN ACCESS

Edited by:
Chris Dupont,
J. Craig Venter Institute, United States

Reviewed by:
Nadine Schubert,
University of Algarve, Portugal
Gang Li,
South China Sea Institute of Oceanology (CAS), China

***Correspondence:**
Kazuhiro Yoshida
sv8269@cc.saga-u.ac.jp
Andrew McMinn
Andrew.McMinn@utas.edu.au
Koji Suzuki
kojis@ees.hokudai.ac.jp

†Present address:
Kazuhiro Yoshida,
Graduate School of Agriculture, Saga University, Saga, Japan

Specialty section:
This article was submitted to Aquatic Microbiology, a section of the journal Frontiers in Marine Science

Received: *22 November 2020*
Accepted: *19 February 2021*
Published: *22 March 2021*

Citation:
Yoshida K, Seger A, Corkill M, Heil P, Karsh K, McMinn A and Suzuki K (2021) Low Fe Availability for Photosynthesis of Sea-Ice Algae: Ex situ Incubation of the Ice Diatom Fragilariopsis cylindrus in Low-Fe Sea Ice Using an Ice Tank. Front. Mar. Sci. 8:632087. doi: 10.3389/fmars.2021.632087

adapt to environmental changes during ice melt under low Fe conditions. Although ice algae can optimize their photosynthesis to sea-ice environments, chronic Fe starvation led to less flexibility of photoacclimation, particularly in low light conditions. This may have detrimental consequences for ice algal production and trophic interactions in sea-ice ecosystems if the recent reduction in sea-ice extent continues.

Keywords: sea-ice diatom, pack ice, iron limitation, ice-edge bloom, Southern Ocean, chlorophyll *a* fluorescence, gene expression, photoprotection

INTRODUCTION

Sea ice is one of the largest biomes on Earth and a significant driver of the biogeochemistry of polar oceans (Arrigo, 2017; van Leeuwe et al., 2018). Sea ice harbors diverse and productive microbial communities that occur mainly at the bottom of sea ice (Meiners et al., 2012, 2018; van Leeuwe et al., 2018). Ice algae, sympagic microalgae proliferating near the bottom of sea ice, are a major primary producer, estimated to contribute 9–25% of the annual primary production (*PP*) in perennial ice zones (e.g., Legendre et al., 1992; Arrigo et al., 1997; Arrigo, 2017). In addition, they also contribute more than 50% of the total *PP* in ice-covered zones (Satoh et al., 1989; McMinn et al., 2010; Fernández-Méndez et al., 2015). When sea ice melts, algal cells are released from the sea ice and can seed extensive ice-edge microalgal blooms (Smith and Nelson, 1986; Syvertsen, 1991). Ice algae therefore are a significant player in the ecology and biogeochemistry of sea ice and marginal ice zones. However, sea ice is a challenging environment for photosynthesis due to low temperatures, high salinities, low light availability, and reduced access to nutrients. In these conditions, light and nutrient availability effectively control photosynthesis in ice algae, although salinity stress can also be important. Pankowski and McMinn (2008) first reported iron (Fe) limitation in Antarctic pack ice in spring/summer. They suggested that it was due to the low Fe supply from the Fe-deficient surface waters of the Southern Ocean, where off the continental shelf, the average concentration of dissolved Fe (DFe), which is considered the most bio-available form (Lannuzel et al., 2014), is 0.31 ± 0.45 nM (Tagliabue et al., 2012). It is well-known that Fe is a crucial element for photosynthesis in microalgae, as it is required for pigments and cytochrome synthesis, nitrate reduction, and the detoxification of reactive oxygen species (ROS) (Geider and LaRoche, 1994; Sunda and Huntsman, 1995; Behrenfeld and Milligan, 2013; Twining and Baines, 2013). Ice algae are able to acclimate to the dark environment frequently encountered in sea ice by increased synthesizing of chlorophylls and carotenoids to maximize the efficiency of light utilization (e.g., Falkowski and Owens, 1980; Morel and Bricaud, 1981; Bricaud et al., 1995). However, pigment synthesis requires Fe; the low availability of Fe can thus be exacerbated due to the antagonistic Fe-light co-limitation (i.e., more Fe required in a darker environment; Sunda and Huntsman, 1997; Maldonado et al., 1999; Moore et al., 2007). The reduced cellular chlorophyll *a* and accessory carotenoids due to Fe-limited conditions (e.g., Greene et al., 1992; Behrenfeld and Milligan, 2013) would lead to serious photo-damage by ROS because Fe-limited cells cannot cope with the excess absorbed energy that overruns the reduced electron transport capacity due to decreased Fe-containing electron donors (e.g., cytochromes and Photosystem I; van Oijen et al., 2004; Petrou et al., 2014; Roncel et al., 2016). This would pose a significant challenge when Fe-limited ice algal cells are exposed to high light during release from the bottom of the sea ice into open waters during ice melt (i.e., the setting of ice-edge blooms). It is thus ecologically and biogeochemically important to investigate how Fe availability and light combine to control the photosynthetic performance of ice algae to further understand their role in sea-ice and marginal ice-zone ecosystems.

Sea ice can act as a reservoir of Fe, especially close to lithogenic coastal iron sources in the case of fast ice (e.g., de Jong et al., 2013), but also in pack ice far from the coast (Lannuzel et al., 2016b). Pack ice might accumulate biogenic Fe by directly incorporating it during growth in autumn and winter (Lannuzel et al., 2016a) or by transferring DFe from seawater into particulate Fe (PFe) (e.g., van der Merwe et al., 2011). According to the limited data available, pack-ice DFe concentrations range from about 0.2–36.8 nM (average 5.9 ± 6.2 nM from 40 cores; Lannuzel et al., 2007, 2008, 2016a; van der Merwe et al., 2011; de Jong et al., 2015; Janssens et al., 2016), up to about two orders of magnitude greater than the underlying seawater (Tagliabue et al., 2012). When sea ice melts in spring and summer, 70% of the DFe can be lost within 10 days (Lannuzel et al., 2008), but PFe, which is about an order of magnitude greater in average concentration, needs to be physically released from both the ice, and gel-like exopolymeric substances (EPS) lining the brine network (Krembs et al., 2002; van der Merwe et al., 2011; Lannuzel et al., 2013, 2016b). These gel-like EPS are produced *in situ* by sea-ice organisms in response to the evolving sea-ice environment and could in turn control the solubility of Fe transferred back to the dissolved fraction (Thomas and Dieckmann, 2002; Lannuzel et al., 2015, 2016b; Genovese et al., 2018), possibly maintaining in-ice DFe within the concentration range described.

With regard to climate change, it has been reported that ocean acidification (OA), associated with the increasing anthropogenic CO_2 input, modifies Fe availability (Millero et al., 2009). OA can suppress Fe availability by stabilizing Fe-ligand complexation (Sunda and Huntsman, 2003; Shi et al., 2010) and also extending the oxidation rate of Fe(II), which is believed to be the most prolific bio-available source of Fe (Millero et al., 1987, 2009; Breitbarth et al., 2009). Although Boyd et al. (2015) estimated that climate change enhances Fe availability in the Southern Ocean, sea ice has greater fluctuations in pH than in pelagic waters (Matson et al., 2014; McMinn et al., 2014). In addition, future predictions of sea-ice algal biomass and photosynthesis in

the changing polar oceans are one of the major missing pieces in sea-ice biogeochemical models (Vancoppenolle et al., 2013; Constable et al., 2014; Steiner et al., 2016; van Leeuwe et al., 2018). Recently, Tedesco et al. (2019) has demonstrated future changes in algal productivity in the Arctic combining a biogeochemical model for sympagic algae with sea-ice drivers from an ensemble of 18 CMIP5 climate models. However, little is known about temporal changes in sea-ice algal biomass and productivity in the changing Southern Ocean.

Methodological limitations to the investigation of ice-algal photosynthesis, however, still remain—almost all studies so far have worked on ice algal photosynthesis in the laboratory, during which ice algae are resuspended in a water medium after being melted out from ice samples. This melt process hinders obtaining realistic photophysiological information because water media cannot reproduce the temperatures in sea ice (<−1.8°C). Kennedy et al. (2012) and Kameyama et al. (2020) successfully incubated ice algae in artificial sea ice produced in laboratory ice tanks. Ice tank techniques enable *ex situ* incubation of ice algae within ice and manipulation of the ice environment by maintaining a stable ice thickness. Yoshida et al. (2020) also incubated the model polar diatom *Fragilariopsis cylindrus* under Fe-replete condition ([total dissolvable Fe] = 400 nM) in artificial ice using an ice tank. Our previous study suggested that ice diatoms, with high Fe availability, flexibly acclimated their physiology to the dynamic ice environments described above. However, photosynthetic responses of ice algae to low Fe availability have not been well-understood yet. Here, we use a newly developed low-Fe ice tank, made of titanium, to control Fe concentration in the ice. Using this novel low-Fe ice tank, we attempted to investigate how low Fe availability in sea ice affects the photosynthetic plasticity of ice algae exposed to dynamic fluctuations in light availability, from extremely low light when sea ice is present, to intense light exposure during the ice melts. Here, the polar diatom *F. cylindrus*, a model ice diatom with a fully sequenced genome, was used (Mock et al., 2017), enabling the application of molecular techniques to understand the underlying mechanisms driving photophysiology. Photophysiological responses of *F. cylindrus* were monitored with variable chlorophyll (chl) *a* fluorescence and their pigment composition throughout the ice tank experiments.

MATERIALS AND METHODS

Ice Tank Incubation and Preparation of Low-Fe Medium

The polar pennate diatom *Fragilariopsis cylindrus*, isolated from Antarctic pack ice in 2015 at Davis Station, East Antarctica (Kennedy et al., 2019), was incubated in a purpose-designed low-Fe ice tank (Island Research, Tasmania; see details in Yoshida et al., 2020). The low-Fe ice tank, which was constructed of titanium to minimize Fe contamination, was placed into a freezer (–20°C). Ice thickness and temperature gradient were controlled by interactions between a basal heater and the adjustable ambient freezer temperature. This enabled an ice thickness of approximately 5.5 cm to be maintained during the experiment. Incubations were conducted in Aquil media (Price et al., 1989; Pankowski and McMinn, 2009; Yoshida et al., 2020) buffered with ethylenediaminetetraacetic acid (EDTA) (final concentration 20 μM) at a salinity of 35 and at 150 and 30 μmol photons m^{-2} s^{-1} (PAR; white LED, PANEL-300-18W; LED Lighting Products, Sydney, NSW, Australia) as high light (HL) and low (LL) treatments, respectively. The diatom was pre-incubated in the same low-Fe Aquil media at 2.5°C and 150 μmol photons m^{-2} s^{-1} before inoculation of the ice tank. DFe concentrations were set at 20 nM, which is within the concentration range of 0.2–36.8 nM that has been found in pack ice (Lannuzel et al., 2007, 2008, 2016a; van der Merwe et al., 2011; de Jong et al., 2015; Janssens et al., 2016), where the concentrations of total inorganic forms of Fe (Fe′) were 4.0 pM calculated using the software Visual MINTEQ, ver. 3[1]. Pankowski and McMinn (2009) confirmed, with Fe-related protein analysis, that low Fe stress was evident at 15.5 pM of Fe′. Two independent ice tank runs were conducted for each light treatment. Results of the low-Fe ice tank runs were compared with those from Fe-replete ice tank experiments ([DFe] = 400 nM) of Yoshida et al. (2020).

The low-Fe experiment commenced with the incubation of *F. cylindrus* in seawater at 2.5°C after 3-day acclimation to the ice tank environment. A seawater sample was obtained to assess the original physiological state of the algae (day-05, hereafter). A freezing cycle was then started by setting the ice tank to −1.8°C to initiate ice formation. When ice had formed on day 2, the under-ice water was partially replaced with ultrapure water to adjust the salinity to 35; because the brine rejection from sea ice had increased the salinity to ∼38. After a 2-day acclimation to the new salinity, ice samples were obtained every 5 days for 20 days (i.e., days 0, 5, 10, 15, and 20; **Figure 1**). Ice samples were randomly recovered with a trace metal-free hand drill (2 cm in diameter) to minimize the heterogeneity among the samples (Yoshida et al., 2020). After all ice sampling at day 20, the remaining ice in the tank was completely melted at 2.5°C to assess the stress of ice melt and high light exposure at 800 μmol photons m^{-2} s^{-1} using the white LED panel (hereafter Melt and Light samples, respectively) (**Figure 1**). The ice tank incubation procedures are shown in Yoshida et al. (2020). Because it was difficult to obtain the concentrations of macro-nutrient samples from the thin artificial ice (5.5 cm), macro-nutrient concentrations of under-ice seawater were measured. It was assumed that the under-ice seawater was the only nutrient source for ice algae in the ice tank. An unstable brine salinity profile and brine volume fractions in excess of percolation threshold (shown in Yoshida et al., 2020) indicated that brines should have been exchanging with the under-ice seawater (Golden et al., 1998). At the beginning and end of the ice tank runs (days −05 and Melt, respectively), concentrations of nitrate and phosphate in under-ice seawater were determined using a QuickChemR 8000 Automated Ion Analyzer (LaChat Instruments) (Britton et al., 2019). Silicate concentrations of under-ice seawater were determined following Parsons et al. (1984) with the alternate reductant, L-ascorbic acid (Sigma), using a spectrophotometer

[1]https://vminteq.lwr.kth.se

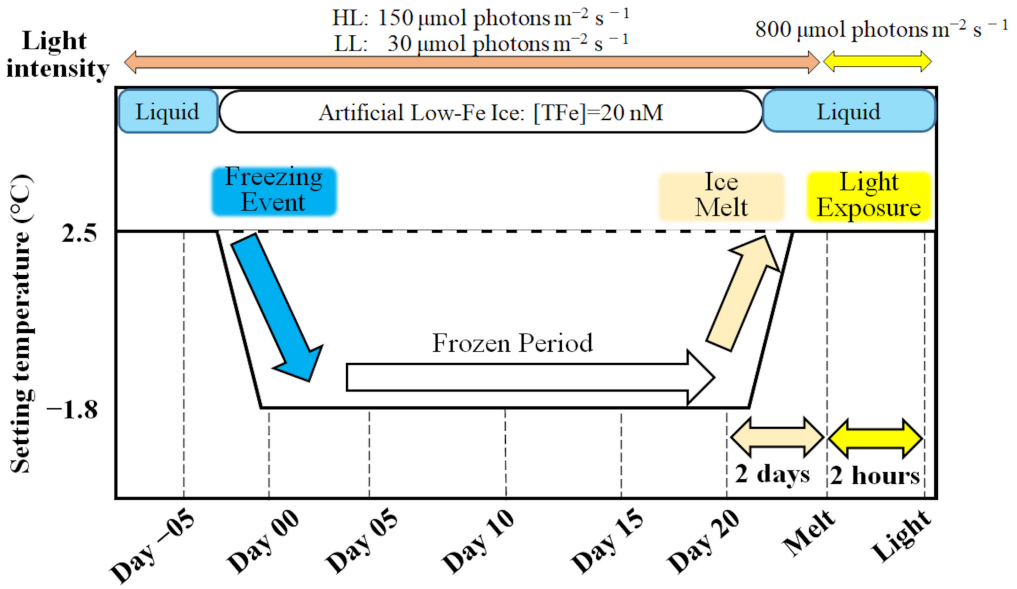

FIGURE 1 | A schematic of the ice tank incubation experiments.

(Model S-22, BOECO). Exponential growth rate (r; d^{-1}) of *F. cylindrus* in the ice was calculated (Wood et al., 2005):

$$\mu = \frac{\ln(N_{Day\ 20} - N_{Day\ 00})}{20}$$

where N_{Day20} and N_{Day00} were algal cell abundance (cells mL^{-1}) at day 20 and day 00, respectively.

Total Dissolvable Fe Concentration

Concentrations of total dissolvable Fe (TDFe) in the under-ice seawater were monitored to check whether contamination by external Fe (e.g., sampling-induced aerosol deposition on the ice) had occurred. Fe concentrations in the ice were difficult to determine because the ice was too thin to obtain a brine sample. In addition, the Fe source for the ice algae in the artificial sea ice would have been restricted to from the under-ice water. Fe concentrations in the water samples were thus determined by the Ferrozine colorimetric method in a laminar flow hood (Stookey, 1970; Farid et al., 2018). Fe samples were placed into a 60 mL low-density polyethylene (LDPE), previously acid-cleaned, bottle (Thermo Fisher Scientific) following the GEOTRACES protocol (Cutter et al., 2017). Fe samples were acidified to pH < 2 with Suprapur HCl (Merck) at least 2 months before the measurements (Farid et al., 2018). A 50 mL ferrozine cocktail was prepared with 10 mM Ferrozine (Sigma), 1.44 M hydroxylamine hydrochloride (Trace metal analysis grade, Wako) and ultrapure water acidified with ultrapure hydrochloric acid (HCl) (Ultrapure grade, Wako). The 0.4 mL of ferrozine cocktail was added to a 20 mL sample. The sample was heated at 70°C for 15 min to accelerate the reduction of Fe(III) to Fe(II) and for detaching Fe(II) from the Fe-EDTA complex. After cooling down the sample, 0.4 mL of an ammonium acetate (Fe analysis grade, Wako) buffer solution, prepared with an ammonia solution (Trace metal grade, Wako), was added to the sample. The buffered sample was incubated at room temperature for 24 h to fully recover Fe in the sample (Farid et al., 2018). Fe concentrations were determined with a spectrophotometer measuring the absorbance of Fe(II)-ferrozine complexes at a wavelength of 562 nm (UV-2450, Shimadzu) with a 50 mm path length glass tube. An Fe standard curve was drawn with a series of known Fe concentrations by diluting an Fe standard solution (Wako) ($r > 0.999$, $n = 7$). The detection limit of the measurement was 10 nM, which was consistent with previous studies (Farid et al., 2018). The quantification limit, defined as 3 SD, was 15 nM.

Ice Structure

Prior to the low-Fe incubation experiments, an ice section was collected to assess the ice structure. Artificial sea ice was produced using the same seawater medium, and a 5 cm × 10 cm × 5.5 cm ice sample was collected from the ice tank using a metal saw. The ice sample was thinned to a 0.5 cm thick vertical section using a band saw (BARNES Junior, BARNCO, Australia) in a −20°C temperature-controlled laboratory. The ice section was planned smooth with a handheld microtome blade before being photographed between cross-polarizing filters. Ice structural measurements were performed in accordance with Langway (1958) and Wongpan et al. (2018).

Fast Repetition Rate (FRR) Fluorometry

A bench-top type Fast Repetition Rate fluorometer (FRRf; FastOcean Act2Run Systems, Chelsea Technologies) was used to monitor the photophysiology of *F. cylindrus* during the ice tank experiments. Variable chlorophyll *a* fluorescence data were processed with Act2Run software (Chelsea Technologies). Melted ice samples were buffered with filtered seawater (FSW) (ice: FSW = 1: 1) at 2°C and kept in the dark for 30 min. Variable

chl *a* fluorescence of the melted ice samples was measured with a single turnover protocol. Briefly, one hundred 2-μs flashlets at a wavelength 450 nm excited reaction centers of PSII (RCII) with 2 μs intervals, and twenty 1-μs flashlets were used for relaxation. Eighteen light steps were applied to generate a rapid light curve (RLC) from 0 to 800 μmol photons m^{-2} s^{-1}. Each step took ∼15 s; one RLC was thus completed in 5 min. To obtain chl *a* fluorescence parameters, six induction and relaxation curves were averaged and fitted to the model of Kolber et al. (1998; **Table 1**). Absolute electron transport rate through the reaction centers of PSII (RCII) (ETR_{RCII}) was calculated as follows:

$$ETR_{RCII} = E \times \sigma_{PSII} \times \frac{F'_q/F'_m}{F_v/F_m} \times \phi_{RCII} \times 6.022 \times 10^{-1}$$

following Suggett et al. (2011) and Schuback et al. (2016), wherein ETR_{RCII} is absolute electron transport rate through RCII, E is actinic light intensity, σ_{PSII} is functional absorption cross section of PSII, the fluorescence ratio was effective quantum yield of PSII photochemistry at E, Φ_{RCII} is the quantum yield of RCII assumed as 1, and the following number is a conversion factor to mol quanta mol $RCII^{-1}$ s^{-1}, respectively. The resultant ETR_{RCII}-E relationship was fitted to the model of Platt et al. (1980) to obtain photosynthesis-irradiance parameters (**Table 1**). We adopted NPQ_{NSV}', non-photochemical quenching based on the normalized Stern-Volmer (S-V) coefficient, to assess the heat dissipation from algal cells following McKew et al. (2013):

$$NPQ'_{NSV} = F'_o/F'_v$$

where F_o' is minimum fluorescence yield after a relaxation sequence following Oxborough and Baker (1997; **Table 1**). NPQ_{NSV}' were measured at the incubation light intensities (i.e., HL: 150 μmol photons m^{-2} s^{-1}; LL: 30 μmol photons m^{-2} s^{-1}) throughout the ice tank experiments.

Pigment Composition

Algal chlorophylls and carotenoids were quantified with Ultra-High Performance Liquid Chromatography (UHPLC) (Suzuki et al., 2015). Fast and directly melted ice samples and seawater samples were filtered onto a 25 mm GF/F filter (Whatman) with gentle vacuum (<0.013 MPa) passing through a 25 mm polypropylene in-line filter holder (Swinnex, Merck). Fast direct melting has little effect on pigment analysis (Rintala et al., 2014; Yoshida et al., 2020). The filter was flash frozen in liquid nitrogen and stored in a deep freezer (−80°C). Prior to the UHPLC pigment quantification, the thawed filter was blotted dry with filter paper and bead-beat in *N*, *N*-dimethylformamide (DMF) to extract pigments (Suzuki et al., 2015). Extracted pigments suspended in DMF were injected into an UHPLC. As an index of photoprotection, ratio of diadinoxanthin (DD) and diatoxanthin (DT) was calculated as DT/(DD + DT), xanthophyll de-epoxidation state (DES) (Katayama and Taguchi, 2013; Katayama et al., 2017; Yan et al., 2019). Biomass of algae was assessed as total chl *a* (Tchl *a*: sum of chl *a*, chlorophyllide *a*, chl *a*-allomer, and chl *a*-epimer) concentrations, whereas contributions of chlorophyllide (chlide) *a* to Tchl *a* were also calculated as an index of breakdown of chl *a*. As indices of photoprotective potentials of

TABLE 1 | Terminology and definition of chlorophyll *a* fluorescence yields using FRRf fluorometry.

Yield and parameter		Unit	Derivation or references
Fluorescence yield			
F	Fluorescence yield	Unitless	
F_o	Minimum fluorescence yield of dark regulated cells	Unitless	
F_m	Maximum fluorescence yield of dark regulated cells	Unitless	
F_v	Maximum variable fluorescence yield	Unitless	F_m-F_o
F'	Fluorescence yield under actinic light	Unitless	
F_o'	Minimum fluorescence yield of actinic light-acclimated cells	Unitless	Oxborough and Baker, 1997
F_m'	Maximum fluorescence yield of actinic light-acclimated cells	Unitless	
F_v'	Variable fluorescence yield under actinic light	Unitless	F_m'-F_o'
F_q'	Difference in fluorescence yields between F' and F_m'	Unitless	F_m'-F'
Fluorescence parameters in the dark			
σ_{PSII}	Functional absorption cross-section of PSII in the dark	nm^2 $RCII^{-1}$	Kolber et al., 1998
F_v/F_m	Maximum quantum yield of PSII photochemistry	Unitless	$(F_m–F_o)/F_m$
τ	Time constant for Q_A reoxidation	ms	Kolber et al., 1998
Fluorescence parameters under actinic light			
$F_q'/F_{m'}$	Effective photochemical efficiency of PSII under actinic light	Unitless	$(F_m'–F')/F_m'$
NPQ_{NSV}'	Non-photochemical quenching based on the S-V approach	Unitless	McKew et al., 2013
ETR_{RCII}-E curve parameters			
ETR_{RCII}	Absolute electron transport rate through RCII	mol e^- mol $RCII^{-1}$ s^{-1}	Schuback et al., 2016
E	Actinic light irradiance	mol photons m^{-2} s^{-1}	
α	Light utilization index under dim light	(mol e^- $RCII^{-1}$ s^{-1}) (μmol photons m^{-2} s^{-1})$^{-1}$	Platt et al., 1980
β	Light inhibition index under high light	(mol e^- $RCII^{-1}$ s^{-1}) (μmol quanta m^{-2} s^{-1})$^{-1}$	Platt et al., 1980
ETR_{max}	Maximum electron transport rate through RCII	mol e^- mol $RCII^{-1}$ s^{-1}	Platt et al., 1980
E_k	Light saturation index	μmol quanta m^{-2} s^{-1}	Platt et al., 1980

F. cylindrus, the ratio of photoprotective carotenoids (PPC: DD, DT, and β,β-carotene) to photosynthetic carotenoids (PSC: only fucoxanthin here) in diatoms (PPC/PSC) and xanthophyll pool size [(DD + DT)/Tchl *a*] were also calculated.

Gene Expression of Photosynthesis-Related Genes, *psbA* and *rbcL*

Gene expression measurement shows the potential mechanisms of responses to drastic changes such as freezing and melting of sea ice. The two photosynthesis-related genes, *psbA* and *rbcL*, were targeted for gene expression measurements. The *psbA* and *rbcL* genes encode the D1 protein in PSII reaction center and the large subunit of ribulose-1,5-bisphosphate carboxylase/oxygenase (RuBisCO), respectively. To stabilize the RNA, RNAlater (Sigma) was immediately added to the ice core after collection. Melted ice and seawater samples were filtered onto two 25 mm, 2 μm polycarbonate Isopore membrane filters (Millipore) with gentle vacuum (<0.013 MPa) passing through a 25 mm polypropylene in-line filter holder (Swinnex, Merck). RNA samples were suspended in 600 μL RLT buffer (Qiagen) in a cryotube, to which 10 μL of β-mercaptoethanol (Sigma-Aldrich) was added. Both RNA and DNA samples were placed in a cryotube, flash frozen in liquid nitrogen and stored in a deep freezer (−80°C). DNA was extracted following Endo et al. (2013), and RNA was extracted following Endo et al. (2015). The extracted RNA was reverse transcribed to complementary DNA (cDNA) with the PrimeScriptTM RT Master Mix (RR036, Takara) reagent according to the manufacturer's specification. Quantitative PCR (qPCR) and quantitative reverse-transcribed PCR (qRT-PCR) were performed to determine the copy number of DNA and cDNA, respectively. Gene expression of the *psbA* and *rbcL* genes were calculated as a ratio of cDNA/DNA. The primer sets and PCR conditions are shown in **Supplementary Table S1**.

Statistical Analysis

Statistical analyses were conducted using the SigmaPlot software program ver. 11.0 (SysStat Software, Inc., San Jose, CA, United States). One-way ANOVA with Tukey's test was performed on obtained data. Variations in a parameter were tested at the individual sampling time point in each light treatment. A difference in a parameter was regarded as significant if $p < 0.05$. Additionally, two-way ANOVA with Tukey's tests was also performed at individual sampling time points between light treatments to identify variations in the parameters if no interaction between light availabilities and sampling time points was observed. The results of two-way ANOVA tests were also found in **Supplementary Table S2**. Shapiro–Wilk's and Levene's tests were performed to confirm the normality and equal variance of the data after normalization with the R statistical software using the package MASS. No statistical analysis was conducted for the results of the Fe-replete ice tank experiments, which were shown for comparison with this low-Fe study. Statistical results of the Fe-replete ice tank runs can be found in Yoshida et al. (2020).

RESULTS

Ice Physics and Ice Algal Growth

The ice thickness was stable at 5.5 cm with little basal ice melting or sublimation of ice from the ice-air interface. During the experiments, the temperature within the ice matrix increased from the ice-air interface (−22.5°C) to the ice-water interface (−2.2°C), and seawater temperature beneath was maintained at ∼ −1.8°C throughout the incubations, as also found in Yoshida et al. (2020). The artificial sea ice growth had commenced with the settling out of individual frazil crystals at the surface of the cooled water column. This layer of fine crystals accumulated to a thickness of 1 cm before downward-growing larger crystals were quickly geometrically selected which favored downward growth. Indeed, the latter resembled columnar ice growth and contained brine channels and pockets (**Figure 2**). There were also some incorporated granular crystals, which indicate turbulence, in the under-ice seawater, possibly due to convection driven by the basal heater (**Figure 2**). Convection driven by the basal heater could have minimized the thickness of the boundary layer at the ice-water interface and kept nutrients mixed in the water-column under the ice. Macro-nutrients were not depleted throughout any of the incubations (**Table 2**). During our incubations, a trace amount of Fe was inevitably introduced, but this contamination was considered to be low and negligible (**Table 2**). TDFe concentrations ranged from 11 to 43 nM, which were equivalent to 2.2 and 8.7 pM of Fe′, respectively. Initial Fe concentrations

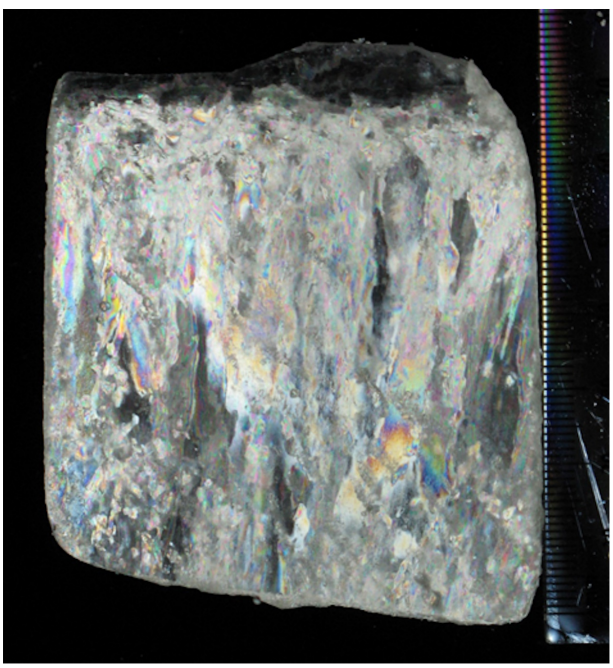

FIGURE 2 | An ice section (0.5 cm thick) of artificial sea ice from the low-Fe ice tank. An ice block (5 cm × 10 cm × 5.5 cm) was sectioned to 0.5 cm with a band saw at −20°C. After planning with a microtome blade, the thick section was photographed between cross-polarized filters.

TABLE 2 | Concentrations of macronutrients, total dissolvable Fe (TDFe), and inorganic Fe species (Fe′).

Treatment	Day	$NO_3 + NO_2$ (μM)	PO_4 (μM)	SiO_4 (μM)	TDFe (nM)	Fe′ (pM)
HL	D-05	290.7 ± 0.1	8.4 ± 0.0	71.3 ± 0.5	23 ± 25	4.6 ± 5.0
	D00	–	–	–	32 ± 0	6.5 ± 0.0
	D05	–	–	–	22 ± 15	4.4 ± 3.1
	D10	–	–	–	38 ± 32	7.6 ± 6.5
	D15	–	–	–	22 ± 15	4.4 ± 3.0
	D20	–	–	–	27 ± 8	5.4 ± 1.5
	Melt	189.8 ± 0.5	5.9 ± 0.0	14.3 ± 0.1	27 ± 8	5.4 ± 1.5
LL	D-05	297.1 ± 0.1	8.9 ± 0.0	86.6 ± 0.5	20 ± 0	4.1 ± 0.0
	D00	–	–	–	22 ± 0	4.3 ± 0.0
	D05	–	–	–	43 ± 22	8.7 ± 4.4
	D10	–	–	–	22 ± 0	4.4 ± 0.0
	D15	–	–	–	33 ± 39	6.6 ± 7.9
	D20	–	–	–	22 ± 15	4.4 ± 3.1
	Melt	264.3 ± 0.8	5.4 ± 0.0	13.2 ± 0.1	25 ± 0	5.1 ± 0.0

Concentrations of macronutrients ($NO_3 + NO_2$, PO_4, SiO_4) were determined with an autoanalyzer (Britton et al., 2019) and a spectrophotometer (Parsons et al., 1984). TDFe concentrations were determined with the Ferrozine method (Stookey, 1970; Farid et al., 2018). The quantification limit of TDFe was 15 nM. Fe′ was calculated with the software Visual MINTEQ, ver 3.1.

No significant variation in TDFe concentration was observed throughout the low-Fe ice tank incubation experiments [One-way ANOVA, $F_{(6,\ 13)} = 0.52$, $p < 0.05$].

were 23 nM and 20 nM (Fe′ = 4.5 and 4.0 pM), while final TDFe concentrations in under-ice seawater were 27 and 25 nM (Fe′ = 5.4 and 5.1 pM) for HL and LL treatments, respectively. No significant variation in Fe concentration during the incubations was observed in either treatment ($p > 0.05$). *F. cylindrus* was certainly incorporated into the ice, and they showed slow but constant positive growth in both light treatments within the ice environments (HL: 0.022 ± 0.006; LL: 0.019 ± 0.009 d^{-1}), showing no significant difference in growth rate between the light treatments (Welch's *t*-test, $t = 0.41$, $p > 0.05$).

Variable Chl *a* Fluorescence

Dark Values (F_v/F_m and σ_{PSII})

At the beginning of the incubations on day −05, planktonic *F. cylindrus* showed relatively low F_v/F_m values (HL: 0.32 ± 0.03; LL: 0.31 ± 0.01) (**Figures 3A,B**). Once algal cells were frozen into the ice, F_v/F_m gradually dropped to <0.2 until day 05 and showed significantly lower values than before ice formation, regardless of light environment (HL: $q = 21.98$, $p < 0.001$; LL: $q = 12.58$, $p < 0.001$) (**Figures 3A,B**). During the frozen period after day 05, F_v/F_m showed stable values at ∼0.2 in both light treatments. When the ice melted, the F_v/F_m values recovered to the values before ice formation at day −05, whereas light exposure to the melted samples significantly decreased the F_v/F_m (HL: 18% decreased; LL: 30% decreased, HL: $q = 6.31$, $p = 0.002$; LL: $q = 11.11$, $p < 0.001$). Both treatments showed an identical σ_{PSII} value at day −05 (HL: 7.41 ± 0.09; 7.53 ± 0.22, Welch's test, $t = 0.874$, $p > 0.05$). In the HL incubation, the σ_{PSII} was stable until day 05 ($q = 2.70$, $p > 0.05$), whereas that in the LL treatment significantly decreased at day 05 compared to day −05 ($q = 6.18$, $p = 0.002$) (**Figures 4A,B**). After day 05, σ_{PSII} gradually increased and reached quite high values near the end of the ice incubation (HL: 9.59 ± 0.44; LL: 10.66 ± 1.96). After the ice melt, σ_{PSII} did not change and rather reflected the values at day 20 (HL: $q = 1.02$, $p > 0.05$; LL: $q = 2.31$, $p > 0.05$) (**Figures 4A,B**). The responses of σ_{PSII} to light exposure were also minimal (HL: $q = 0.71$, $p > 0.05$; LL: $q = 1.75$, $p > 0.05$; **Figures 4A,B**), being different from those of F_v/F_m.

Non-photochemical Quenching (NPQ_{NSV}')

Non-photochemical quenching (NPQ_{NSV}') was relatively high at the initial stage on day −05 (**Figures 5A,B**). Freezing enhanced NPQ_{NSV}' in the HL treatment ($q = 5.14$, $p = 0.016$), whereas no significant change was observed in the LL treatment ($q = 2.49$, $p > 0.05$). However, NPQ_{NSV}' was also significantly upregulated in the early stage of the frozen period at day 05 in the LL treatment ($q = 5.55$, $p = 0.008$). In addition, NPQ_{NSV}' was gradually upregulated and reached plateaus in both light treatments (**Figures 5A,B**). After the ice melt, NPQ_{NSV}' decreased to similar levels observed on day −05 in both light treatments, while light exposure to the melted samples led to different responses between the HL and LL treatments. Light exposure to the melted samples from the HL treatment little affected NPQ_{NSV}' ($q = 3.16$, $p > 0.05$), whereas the NPQ_{NSV}' in the LL treatment was upregulated upon light exposure ($q = 6.25$, $p = 0.002$).

Photosynthesis-Irradiance (ETR_{RCII}-*E*) Curve

The initial slopes of ETR_{RCII}-*E* curves; α, regarded as light utilization efficiency, did not exhibit any change as the *F. cylindrus* cells were integrated into the freezing ice matrix (**Figures 6A,B**). During the frozen periods, α values gradually and constantly increased under both HL and LL conditions. The ice melt event decreased α values to the initial levels. The light exposure did not change α (**Figures 6A,B**) (HL: $q = 0.47$, $p > 0.05$; LL: $q = 0.77$, $p > 0.05$). Maximum electron transport rates (ETR_{max}) showed significant decreases in both treatments during the frozen period compared with the initial ETR_{max} values

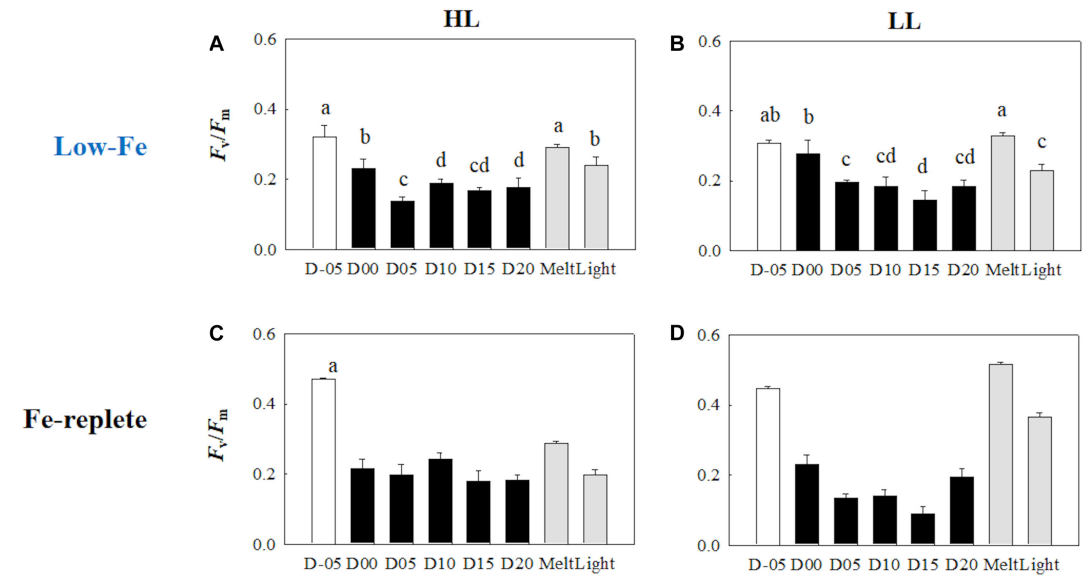

FIGURE 3 | Maximum photochemical quantum yield of PSII (F_v/F_m) at each sampling time point during the ice tank incubation experiments. Panels **(A,B)** show F_v/F_m values of the low-Fe ice tank runs in this study, whereas panels **(C,D)** show those of Fe-replete ice tank runs modified from Yoshida et al. (2020). Left **(A,C)** and right **(B,D)** panels indicate data from the HL and LL treatments, respectively. Open, closed, and shaded bars indicate values of pre-freeze seawater, ice, melted seawater samples, respectively. Letters above bars in a panel indicate significant differences in values between sampling days with one-way ANOVA with Tukey's test; there is no significant difference between values if a given letter is shown in the combination of letters of the counterparts. The D stands for "day," while Melt and Light indicate values after melting and light exposure experiments, respectively. Error bars show 1 standard deviation (n = 6). One-way ANOVA with Tukey's test, HL: $F_{(7,\ 47)} = 57.53$, $p < 0.001$; LL: $F_{(7,\ 47)} = 55.64$, $p < 0.001$; Two-way ANOVA test with Tukey's test, Light: $F_{(1,\ 90)} = 0.0254$, $p > 0.05$; Day: $F_{(7,\ 90)} = 24.88$, $p < 0.001$; Light*Day: $F_{(7,\ 90)} = 3.05$, $p = 0.007$. The results of Tukey's test, as q-values, are given in the text.

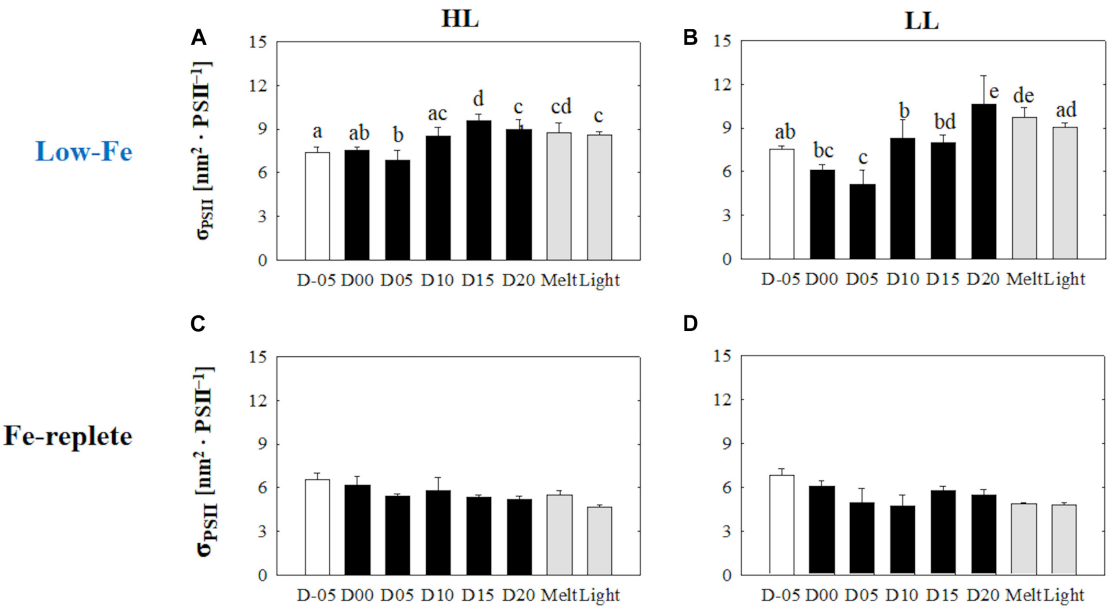

FIGURE 4 | Functional absorption cross-section of PSII (σ_{PSII}) at each sampling time point during the ice tank incubation experiments. Panels **(A,B)** show σ_{PSII} values of the low-Fe ice tank runs in this study, whereas panels **(C,D)** show those of Fe-replete ice tank runs modified from Yoshida et al. (2020). Left **(A,C)** and right **(B,D)** panels indicate data from the HL and LL treatments, respectively. Open, closed, and shaded bars indicate values of pre-freeze seawater, ice, melted seawater samples, respectively. Letters above bars in a panel indicate significant differences in values between sampling days and light treatments with one-way/two-way ANOVA with Tukey's test; there is no significant difference between values if a given letter is shown in the combination of letters of the counterparts. The D stands for "day," while Melt and Light indicate values after melting and light exposure experiments, respectively. Error bars show 1 standard deviation (n = 6). One-way ANOVA with Tukey's test, HL: $F_{(7,\ 47)} = 18.80$, $p < 0.001$; LL: $F_{(7,\ 47)} = 21.98$, $p < 0.001$. Two-way ANOVA test with Tukey's test, Light: $F_{(1,\ 90)} = 1.37$, $p > 0.05$; Day: $F_{(7,\ 90)} = 20.04$, $p < 0.001$; Light*Day: $F_{(7,\ 90)} = 2.13$, $p > 0.05$. The results of Tukey's tests, as q-values, are given in the text.

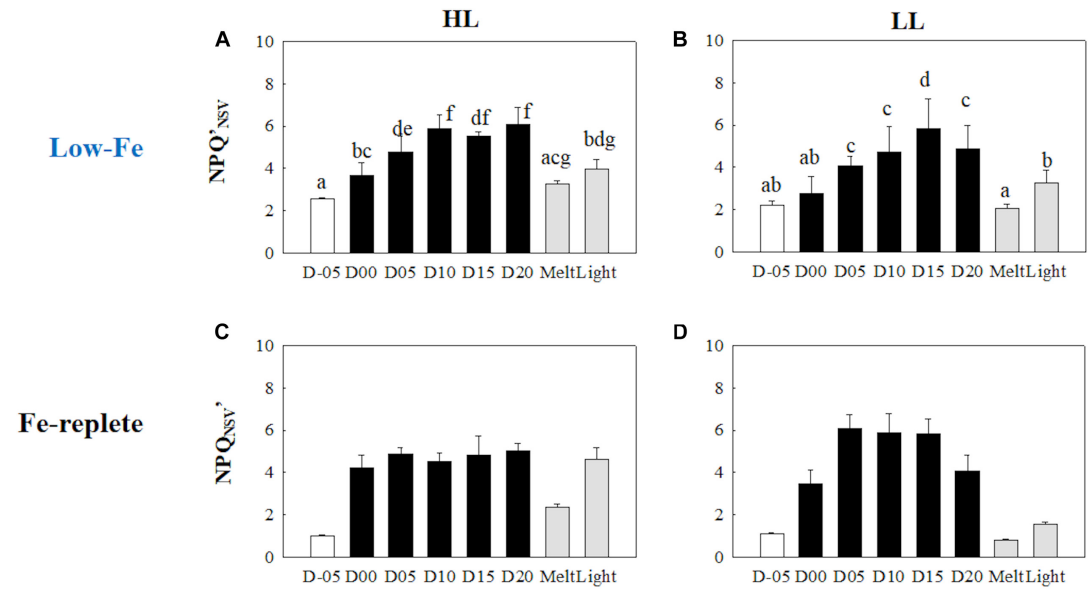

FIGURE 5 | Non-photochemical quenching based on the normalized Stern-Volmer quenching coefficient under the actinic light (150 and 30 μmol photons m^{-2} s^{-1} for HL and LL, respectively) (NPQ_{NSV}') at each sampling time point during the ice tank incubation experiments. Panels **(A,B)** show NPQ_{NSV}' values of the low-Fe ice tank runs in this study, whereas panels **(C,D)** show those of Fe-replete ice tank runs modified from Yoshida et al. (2020). Left **(A,C)** and right **(B,D)** panels indicate data from the HL and LL treatments, respectively. Open, closed, and shaded bars indicate values of pre-freeze seawater, ice, melted seawater samples, respectively. Letters above bars in a panel indicate significant differences in values between sampling days with one-way ANOVA with Tukey's test; there is no significant difference between values if a given letter is shown in the combination of letters of the counterparts. The D stands for "day," while Melt and Light indicate values after melting and light exposure experiments, respectively. Error bars show 1 standard deviation (n = 6). One-way ANOVA with Tukey's test, HL: $F_{(7,\ 47)} = 36.03$, $p < 0.001$; LL:. $F_{(7,\ 47)} = 29.12$, $p < 0.001$. Two-way ANOVA test with Tukey's test, Light: $F_{(1,\ 75)} = 24.40$, $p < 0.001$; Day: $F_{(7,\ 90)} = 45.74$, $p < 0.001$; Light*Day: $F_{(7,\ 90)} = 34.49$, $p < 0.001$. A significant interaction between the light availabilities and sampling time points was observed. The results of Tukey's test, as q-values, are given in the text.

(**Figures 7A,B**) (HL: $q < 6.28$, $p < 0.01$; LL: $q < 10.05$, $p < 0.001$). However, the ice algal cells in the HL sustained the initial ETR_{max} values at the beginning of the frozen period at day 00 ($q = 2.36$, $p > 0.05$). Once the ice had melted, ETR_{max} values recovered to their pre-freezing levels (**Figures 7A,B**); however, light exposure had minimal effects on ETR_{max} (**Figures 7A,B**) (HL: $q = 2.37$, $p > 0.05$; LL: $q = 0.26$, $p > 0.05$). Values of the light saturation index, E_k, first gradually decreased over the course of the incubation experiments but no conspicuous variation was observed after day 05 during the frozen period (HL: $0.45 < q < 2.81$, $p > 0.05$; LL: $0.16 < q < 2.15$, $p > 0.05$, **Figures 8A,B**). Melting increased the E_k values to the initial levels before freezing on day −05, whereas the light exposure did not change the E_k values in either treatment (**Figures 8A,B**) (HL: $q = 2.50$, $p > 0.05$; LL: $q = 1.05$, $p > 0.05$).

Pigment Composition

Initial Tchl *a* concentrations were comparable regardless of light availability (Welch's test, $t = 0.19$, $p > 0.05$, **Figures 9A,B**); however, the LL treatment showed higher Tchl *a* biomass during the frozen period ($q = 6.24$, $p < 0.001$). The contribution of chlide *a* to Tchl *a* gradually increased during the course of the incubations (**Figures 9A,B**). When the cells were exposed to high light after the ice had melted, there were substantial increases in the chlide *a* to Tchl *a* ratio in both light treatments (HL: $q = 7.25$, $p = 0.002$; LL: $q = 5.20$, $p = 0.033$, **Figures 9A,B**). The DD-DT pool size in the HL treatment was significantly higher than that in the LL treatment throughout the incubations ($q = 3.02$, $p = 0.041$; **Figures 10A,B**). The DD-DT pool size at the end of the frozen period at day 20 was significantly higher than the initial size in the HL treatment ($q = 5.05$, $p = 0.041$, **Figure 10A**), whereas no significant change in the pool size was observed in the LL treatment ($p > 0.05$, **Figure 10B**). Values of DES increased slightly later than the algal cells that had been frozen into the ice and remained stable in both light treatments (**Figures 10A,B**). The DES levels decreased when algal cells were melted out in both light treatments (HL: $q = 55.89$, $p < 0.001$; LL: $q = 14.83$, $p < 0.001$). Light exposure did not change the DES levels in the HL treatment ($q = 4.56$, $p > 0.05$, **Figure 10A**); however, the DES in the LL treatment significantly decreased after the light exposure ($q = 5.91$, $p = 0.013$, **Figure 10B**). The HL treatment showed a gradual and sharp increase in PPC/PSC during the frozen period (**Figure 11A**), whereas no conspicuous change was observed in the LL treatment throughout the incubation ($p > 0.05$, **Figure 11B**). When the ice melted, there was a significant decrease in the PPC/PSC in the HL treatment ($q = 5.73$, $p = 0.016$), down to the level prior to the start of the frozen period (**Figure 11A**). The light exposure little affected the PPC/PSC ratios in both light treatments (HL: $q = 0.21$, $p < 0.05$, LL: $p < 0.05$, **Figures 11A,B**). The PPC/PSC level of the HL treatment was significantly higher than that of the LL treatment throughout the incubations ($q = 5.39$, $p < 0.001$).

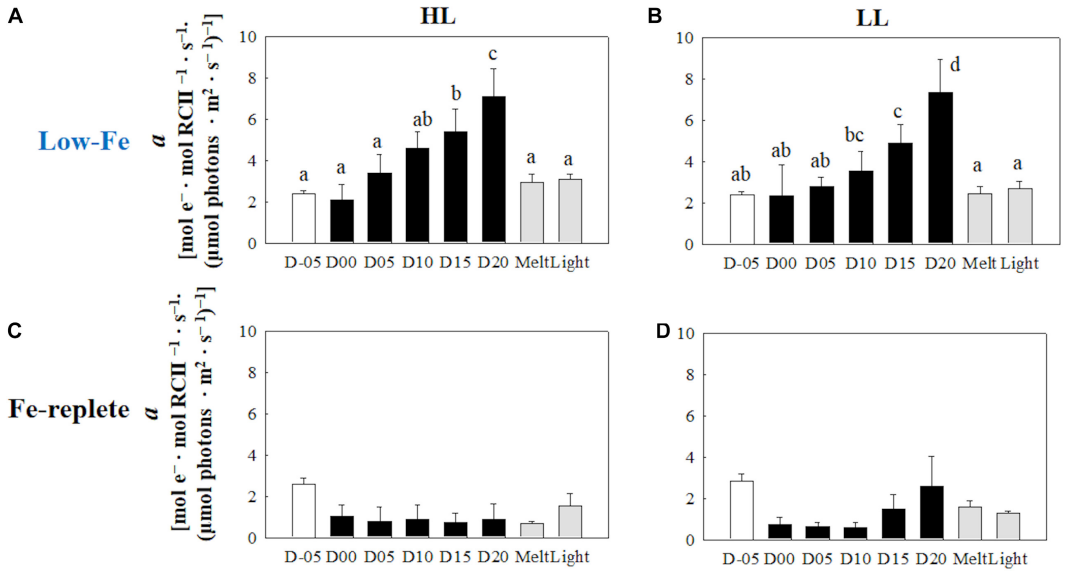

FIGURE 6 | Light utilization index (α) calculated from the photosynthesis-irradiance (ETR_{RCII}-*E*) relationship at each sampling time point during the ice tank incubation experiments. Panels **(A,B)** show α values of the low-Fe ice tank runs in this study, whereas panels **(C,D)** show those of Fe-replete ice tank runs modified from Yoshida et al. (2020). Left **(A,C)** and right **(B,D)** panels indicate data from the HL and LL treatments, respectively. Open, closed, and shaded bars indicate values of pre-freeze seawater, ice, melted seawater samples, respectively. Letters above bars in a panel indicate significant differences in values between sampling days with one-way ANOVA with Tukey's test; there is no significant difference between values if a given letter is shown in the combination of letters of the counterparts. The D stands for "day," while Melt and Light indicate values after melting and light exposure experiments, respectively. Error bars show 1 standard deviation (n = 6). One-way ANOVA with Tukey's test, HL: $F_{(7, 47)}$ = 26.84, $p < 0.001$; LL: $F_{(7, 47)}$ = 21.03, $p < 0.001$. Two-way ANOVA test with Tukey's test, Light: $F_{(1, 90)}$ = 3.68, $p > 0.05$; Day: $F_{(7, 90)}$ = 36.02, $p < 0.001$; Light*Day: $F_{(7, 90)}$ = 0.88, $p > 0.05$. The results of Tukey's test, as q-values, are given in the text.

Gene Expression of Photosynthesis-Related Genes

rbcL

Gene expressions of the *rbcL* gene were highly upregulated when the algal cells were frozen into the ice in both light treatments (HL: q = 9.23, $p < 0.001$; LL: q = 5.14, p = 0.036, **Figures 12A,B**). During the frozen periods, however, gene expression levels dropped sharply (HL: q = 10.39, $p < 0.001$; LL: q = 7.10, p = 0.003), to a lower level than that of the values from the seawater prior to the initiation of freezing (**Figures 12A,B**). The low level was sustained throughout the frozen period. Ice melt also did not affect the transcriptional activity of the *rbcL* gene. In addition, the *rbcL* gene expression did not show any conspicuous changes in either treatment after light exposure (HL: q = 0.44, $p > 0.05$; LL: q = 0.24, $p > 0.05$, **Figures 12A,B**). Interestingly, the HL treatment showed a significantly higher *rbcL* gene expression than the LL treatment throughout the incubations (q = 3.93, p = 0.009).

psbA

Unlike the *rbcL* gene, gene expression of the *psbA* gene behaved differently with differences in light availability (**Figures 13A,B**). Under HL conditions, transcriptional levels of the *psbA* gene dynamically changed; the highest value was observed while algal cells were frozen within the ice matrix (**Figure 13A**). This peak value was significantly higher than the low expression levels at the end of the frozen period (q = 7.17, p = 0.002, **Figure 13A**), which was similar to the *rbcL* variation in the HL treatment (**Figure 12A**). The LL treatment, on the other hand, showed a constant *psbA* gene expression with no significant change ($p > 0.05$) (**Figure 13B**). Both ice melt and light exposure had minimal effects on the transcriptional activity of the *psbA* gene in both light treatments (HL: $q > 1.15$, $p > 0.05$; LL: $p > 0.05$, **Figures 13A,B**).

DISCUSSION

Ice Physics and Chemistry

Our experiments resulted in the first successful incubation of the diatom *Fragilariopsis cylindrus* in artificial sea ice at a low Fe concentration using a purpose-designed low Fe ice tank (**Figure 1**). Our prolonged ice tank runs demonstrated the photophysical responses and competency of the ice algae, *F. cylindrus,* to low Fe availability in the Southern Ocean. The thick section of artificial ice contained elongated brine channels with some brine pockets in the ice matrix, which consisted of frazil ice granules at the top and columnar ice below the upper 1 cm (**Figure 2**). This structure suggests that the ice tank realistically reproduced a natural sea-ice environment (e.g., Petrich and Eicken, 2017). As discussed in our previous work using the same ice tank (Yoshida et al., 2020), the sharp decrease in temperature (top: −22.5°C; bottom: −2.2°C in 5.5 cm) was consistent with the winter-time pack ice environment (Petrich and Eicken, 2017). Macro-nutrients were sufficient to maintain growth throughout the experiments and to ensure that Fe was

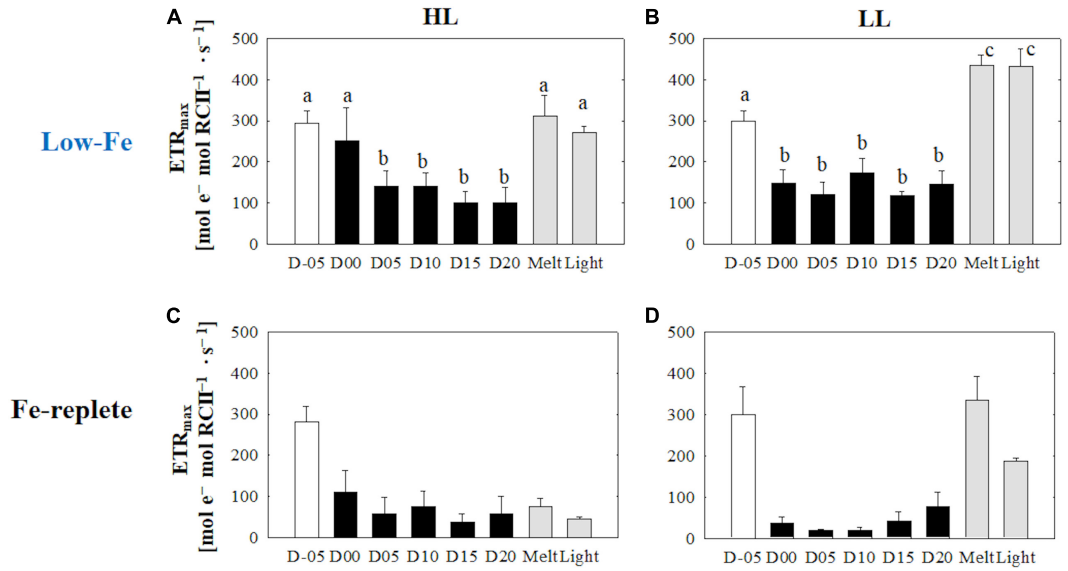

FIGURE 7 | Maximum electron transport rate (ETR_{max}) calculated from the photosynthesis-irradiance (ETR_{RCII}-E) relationship at each sampling time point during the ice tank incubation experiments. Panels **(A,B)** show ETR_{max} values of the low-Fe ice tank runs in this study, whereas panels **(C,D)** show those of Fe-replete ice tank runs modified from Yoshida et al. (2020). Left **(A,C)** and right **(B,D)** panels indicate data from the HL and LL treatments, respectively. Open, closed, and shaded bars indicate values of pre-freeze seawater, ice, melted seawater samples, respectively. Letters above bars in a panel indicate significant differences in values between sampling days with one-way ANOVA with Tukey's test; there is no significant difference between values if a given letter is shown in the combination of letters of the counterparts. The D stands for "day," while Melt and Light indicate values after melting and light exposure experiments, respectively. Error bars show 1 standard deviation (n = 6). One-way ANOVA with Tukey's test, HL: $F_{(7,\ 47)}$ = 25.85, $p < 0.001$; LL: $F_{(7,\ 47)}$ = 118.16, $p < 0.001$. Two-way ANOVA test with Tukey's test, Light: $F_{(1,\ 90)}$ = 10.09, $p > 0.05$; Day: $F_{(7,\ 90)}$ = 35.07, $p < 0.001$; Light*Day: $F_{(7,\ 90)}$ = 6.36, $p < 0.001$. A significant interaction between the light availabilities and sampling time points was observed. The results of Tukey's test, as q-values, are given in the text.

the limiting nutrient. The consistently low Fe′ concentration confirmed that the ice tank runs had been conducted at low Fe levels throughout the experiments (**Table 2**). Although low Fe availability suppressed PSII photochemical efficiency (discussed below in 4.2), the observed growth rates (HL: 0.022 ± 0.006; LL: 0.019 ± 0.009 d^{-1}) were identical to those in Fe-replete ice tanks runs (0.020 d^{-1}; Yoshida et al., 2020). This suggests acclimation to the low Fe condition. Pankowski and McMinn (2008) reported that moderate Fe limitation occurred at ∼5 pM Fe′ for *F. cylindrus*, which is a similar level to that of this study (HL: 4.6-6.5 pM Fe′; LL: 4.1-8.7 pM Fe′; **Table 2**). It is thus suggested that our ice tank incubation experiments were appropriate to assess how freezing and melting stress under chronic Fe starvation affects the photosynthetic physiology of ice algal *F. cylindrus*.

Freezing Event

Freezing stress lowered the photochemical efficiency and stemmed the electron transport. At the beginning of the incubation, F_v/F_m values were reasonably low (∼0.3) (**Figures 3A,B**), which was ca. 30 % lower than the previous Fe-replete ice tank incubation experiments (F_v/F_m = ∼0.45; Yoshida et al., 2020; **Figures 3C,D**). Kolber et al. (1994) and Suzuki et al. (2002) demonstrated that Fe availability affects photochemical reactions at RCII, since PSII has 2 Fe atoms and a high turnover rate (Greene et al., 1992; Geider and LaRoche, 1994; Govindjee et al., 2010). These observations demonstrate that we successfully incubated ice algae under low-Fe conditions for the first time. The freezing event gradually decreased both F_v/F_m and σ_{PSII} values until day 05 (**Figures 3A,B**, **4A,B**). In principle, σ_{PSII} is a function of the optical absorption cross section of PSII ($\sigma^{opt}{}_{PSII}$) and maximal quantum yield of PSII photochemistry ($\Phi^{max}{}_{PSII}$, or F_v/F_m) (e.g., Huot and Babin, 2011):

$$\sigma_{PSII} = \sigma^{opt}_{PSII} \times \sigma^{max}_{PSII}$$

The concomitant decrease thus suggests that the reduced photochemical efficiency of PSII (i.e., F_v/F_m) lowered the σ_{PSII} when *F. cylindrus* cells were frozen into the ice. Also, $NPQ_{NSV}{}'$ gradually increased, while F_v/F_m conversely decreased with the freezing stress (**Figures 3A,B**, **5A,B**), suggesting that the photosynthetic apparatus of *F. cylindrus* was well-protected from freezing stress even under the Fe-starved condition. Although σ_{PSII} decreased (**Figures 4A,B**), the light utilization index, α, did not respond to the freezing event (**Figures 6A,B**). In general, α is a product of σ_{PSII} and the concentration of functional RCII (n_{PSII}):

$$\alpha = \sigma_{PSII} \times n_{PSII}$$

The stable α values suggest that *F. cylindrus* could increase n_{PSII} in response to low-light acclimation (n_{PSII} strategy, hereafter) with freezing stress. However, these were unexpected physiological responses, because it is Fe-costly to synthesize PSII (e.g., Geider and LaRoche, 1994; Twining and Baines, 2013). Interestingly, ETR_{max} maintained higher values (**Figures 7A,B**),

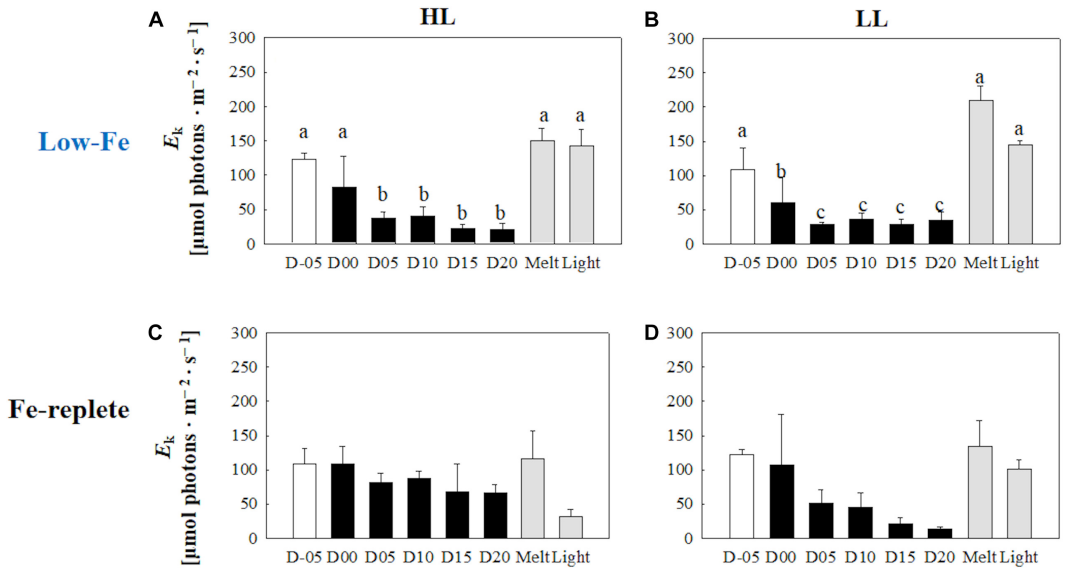

FIGURE 8 | Light saturation index (E_k) calculated from the photosynthesis-irradiance (ETR_{RCII}-E) relationship at each sampling time point during the ice tank incubation experiments. Panels **(A,B)** show E_k values of the low-Fe ice tank runs in this study, whereas panels **(C,D)** show those of Fe-replete ice tank runs modified from Yoshida et al. (2020). Left **(A,C)** and right **(B,D)** panels indicate data from the HL and LL treatments, respectively. Open, closed, and shaded bars indicate values of pre-freeze seawater, ice, melted seawater samples, respectively. Letters above bars in a panel indicate significant differences in values between sampling days with one-way ANOVA with Tukey's test; there is no significant difference between values if a given letter is shown in the combination of letters of the counterparts. The D stands for "day," while Melt and Light indicate values after melting and light exposure experiments, respectively. Error bars show 1 standard deviation (n = 6). One-way ANOVA with Tukey's test, HL: $F_{(7,\ 47)} = 12.88$, $p < 0.001$; LL: $F_{(7,\ 47)} = 41.46$, $p < 0.001$. Two-way ANOVA test with Tukey's test, Light: $F_{(1,\ 90)} = 0.62$, $p > 0.05$; Day: $F_{(7,\ 90)} = 22.86$, $p < 0.001$; Light*Day: $F_{(7,\ 90)} = 1.54$, $p > 0.05$. The results of Tukey's test, as q-values, are given in the text.

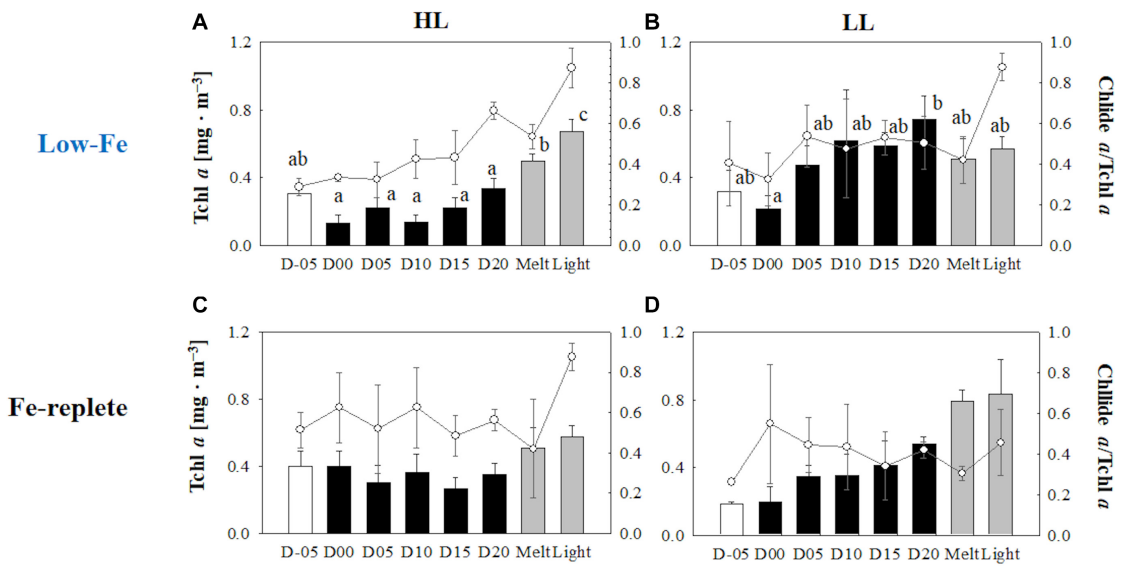

FIGURE 9 | Total chlorophyll *a* (Tchl *a*) concentrations contributions of chlide a to Tchl *a* at each sampling time point during the ice tank incubation experiments. Panels **(A,B)** show Tchl *a* concentrations (bars, left axis) and contributions of chlide *a* to Tchl *a* (open circles, right axis) of the low-Fe ice tank runs in this study, whereas panels **(C,D)** show those of Fe-replete ice tank runs modified from Yoshida et al. (2020). Left **(A,C)** and right **(B,D)** panels indicate data from the HL and LL treatments, respectively. Open, closed, and shaded bars indicate values of pre-freeze seawater, ice, melted seawater samples, respectively. Letters above bars in a panel indicate significant differences in values between sampling days and light treatments with one-way ANOVA with Tukey's test; there is no significant difference between values if a given letter is shown in the combination of letters of the counterparts. The D stands for "day," while Melt and Light indicate values after melting and light exposure experiments, respectively. Error bars show 1 standard deviation (n = 3). Tchl *a*: One-way ANOVA with Tukey's test, HL: $F_{(7,\ 23)} = 24.17$, $p < 0.001$; LL: $F_{(7,\ 23)} = 2.78$, $p = 0.48$; Two-way ANOVA with Tukey's test, Light: $F_{(1,\ 46)} = 19.44$, $p < 0.001$; Day: $F_{(7,\ 46)} = 5.68$, $p < 0.001$; Light*Day: $F_{(7,\ 46)} = 2.15$, $p > 0.05$. Chlide *a*/Tchl *a*: One-way ANOVA with Tukey's test, HL: $F_{(7,\ 23)} = 18.40$, $p < 0.001$; LL: $F_{(7,\ 23)} = 3.53$, $p = 0.017$. Two-way ANOVA test with Tukey's test, Light: $F_{(1,\ 46)} = 1.71$, $p > 0.05$; Day: $F_{(7,\ 46)} = 9.29$, $p < 0.001$; Light*Day: $F_{(7,\ 46)} = 2.40$, $p > 0.05$. The results of Tukey's test, as q-values, are given in the text.

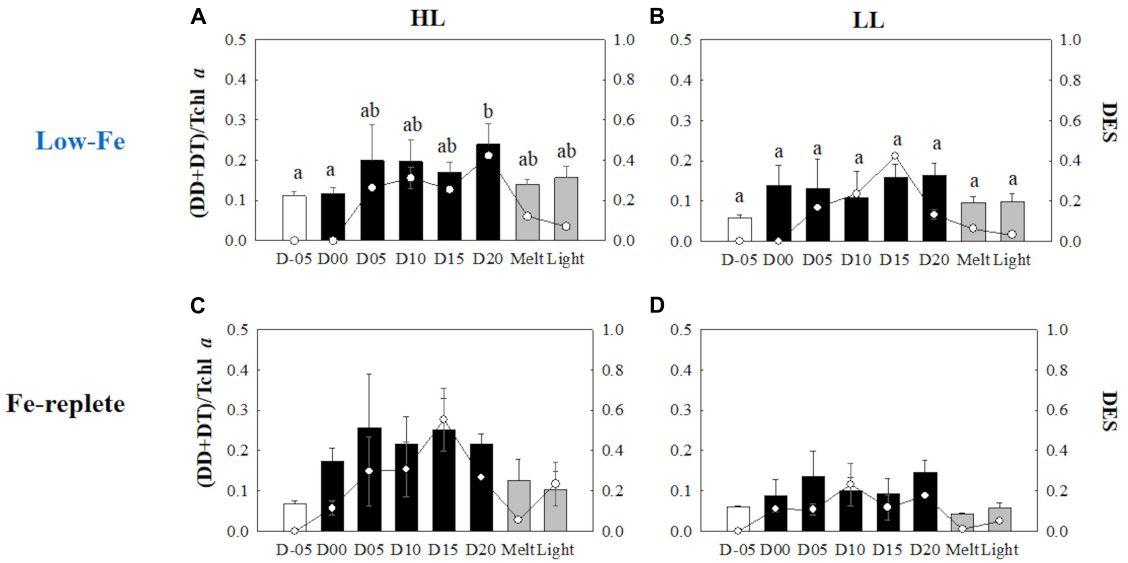

FIGURE 10 | Xanthophyll pool size [(DD + DT)/Tchl *a*] and xanthophyll de-epoxidation states (DES) at each sampling time point during the ice tank incubation experiments. Panels **(A,B)** show xanthophyll pool size (bars, left axis) and DES (markers, right axis) of the low-Fe ice tank runs in this study, whereas panels **(C,D)** show those of Fe-replete ice tank runs modified from Yoshida et al. (2020). Left **(A,C)** and right **(B,D)** panels indicate data from the HL and LL treatments, respectively. Open, closed, and shaded bars indicate values of pre-freeze seawater, ice, melted seawater samples, respectively. Letters above bars in a panel indicate significant differences in values between sampling days and light treatments with one-way/two-way ANOVA with Tukey's test; there is no significant difference between values if a given letter is shown in the combination of letters of the counterparts. The D stands for "day," while Melt and Light indicate values after melting and light exposure experiments, respectively. Error bars show 1 standard deviation (n = 3). Xanthophyll pool size: One-way ANOVA with Tukey's test, HL: $F_{(7,\ 23)} = 3.03$, $p = 0.032$, LL: $F_{(7,\ 23)} = 2.00$, $p > 0.05$; Two-way ANOVA with Tukey's test, Light: $F_{(1,\ 46)} = 4.55$, $p = 0.041$; Day: $F_{(7,\ 46)} = 2.26$, $p > 0.05$; Light*Day: $F_{(1,\ 46)} = 0.40$, $p < 0.05$. DES: One-way ANOVA with Tukey's test, HL: $F_{(7,\ 23)} = 771.14$, $p < 0.001$; LL: $F_{(7,\ 23)} = 188.50$, $p < 0.001$. Two-way ANOVA test with Tukey's test, Light: $F_{(1,\ 46)} = 61.35$, $p < 0.001$; Day: $F_{(7,\ 46)} = 11.51$, $p < 0.001$; Light*Day: $F_{(7,\ 46)} = 14.01$, $p < 0.001$. A significant interaction between the light availabilities and sampling time points was observed. The results of Tukey's test, as q-values, are given in the text.

which were similar to those of the Fe-replete ice tank experiments (Yoshida et al., 2020; **Figures 7C,D**). Schuback et al. (2015) also reported relatively high ETR_{max} values in Fe-limited waters. They hypothesized the existence and upregulation of alternative pathways for electrons to dissipate the excess energy, rather than xanthophyll cycling. These included pseudo-cyclic and cyclic electron flow (Prášil et al., 1996; Feikema et al., 2006; Cardol et al., 2011), which would have reduced the high transmembrane ΔpH under low Fe conditions. The resultant E_k value eventually showed the dark-acclimated state (**Figures 8A,B**). The contribution of chlide *a* to Tchl *a* was stable when cells had frozen into the ice, indicating a smaller effect of the melting process on pigment breakdown and the production of chlide *a* (**Figures 9A,B**). The size of DD-DT pool was also stable, and the xanthophyll cycle had not been activated at day 00 (**Figures 10A,B**). This suggests that other non-photochemical quenching pathways were responsible for the NPQ. However, the xanthophyll cycle activated at day 05 with the upregulation of NPQ_{NSV}', suggesting that diatoms had gradually acclimated to the ice environment by employing their photoprotective capability (**Figures 5A,B**, **10A,B**). Gene expression of the *rbcL* gene were upregulated in both light treatments (**Figures 12A,B**), emphasizing the cold acclimation strategy. The carboxylation rate of RuBisCO critically slows down at low temperatures (Young et al., 2015). The *rbcL* gene upregulation could enhance the synthesis rate of RuBisCO to complement the low enzymatic activity by increasing the cellular enzyme concentration (Devos et al., 1998; Lyon and Mock, 2014; Young et al., 2015; Yoshida et al., 2018). A contrasting response was found for the *psbA* gene, i.e., upregulation in the HL treatment while constant in the LL treatment (**Figures 13A,B**). The upregulation of the *psbA* in the HL treatment could be a strategy to overcome over-excitation associated with HL and possibly the freezing stress causing electron clogging. This upregulation also suggests that the turnover rate of D1 proteins was accelerated due to a higher rate of PSII photodamage.

Frozen Period

Sea ice provides a stable platform for photosynthesis of ice algae, which might optimize their photophysiology in spite of the low Fe availability. Regardless of light intensity, F_v/F_m values during the frozen period were comparable to the previous study under Fe-replete conditions (Yoshida et al., 2020; **Figures 3C,D**). This suggests that both Fe and light availability had little effect on PSII reaction center activity and growth of *F. cylindrus* in the sea-ice environment. Pankowski and McMinn (2008) reported similar growth rates of *F. cylindrus* both in Fe-replete and Fe-starved culturing media. Although F_v/F_m values were stable in our experiments, σ_{PSII} showed gradual increases during the course of the incubation (**Figures 3A,B**, **4A,B**). Interestingly, the other index of light absorption efficiency, α, increased synchronously with σ_{PSII} (**Figures 4A,B**, **6A,B**), suggesting that the increase

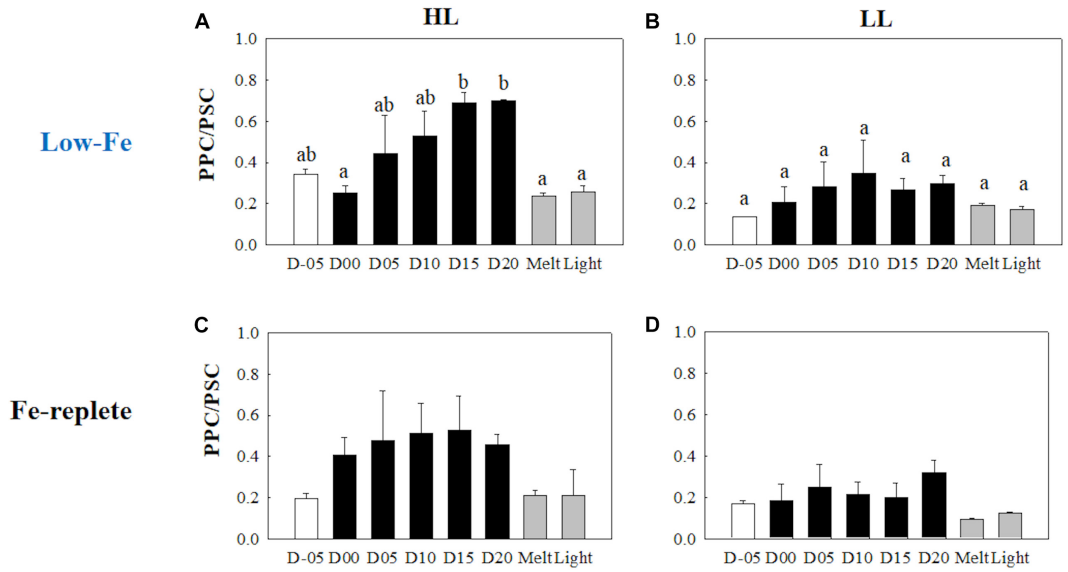

FIGURE 11 | Ratio of Photoprotective to photosynthetic carotenoids (PPC/PSC) at each sampling time point during the ice tank incubation experiments. Panels **(A,B)** show PPC/PSC ratios of the low-Fe ice tank runs in this study, whereas panels **(C,D)** show those of Fe-replete ice tank runs modified from Yoshida et al. (2020). Left **(A,C)** and right **(B,D)** panels indicate data from the HL and LL treatments, respectively. Open, closed, and shaded bars indicate values of pre-freeze seawater, ice, melted seawater samples, respectively. Letters above bars in a panel indicate significant differences in values between sampling days with one-way ANOVA with Tukey's test; there is no significant difference between values if a given letter is shown in the combination of letters of the counterparts. The D stands for "day," while Melt and Light indicate values after melting and light exposure experiments, respectively. Error bars show 1 standard deviation (n = 3). One-way ANOVA with Tukey's test, HL: $F_{(7,\ 23)} = 5.62$, $p = 0.002$; LL: $F_{(7,\ 23)} = 2.39$, $p > 0.05$. Two-way ANOVA test with Tukey's test, Light: $F_{(1,\ 46)} = 14.52$, $p < 0.001$; Day: $F_{(7,\ 46)} = 2.87$, $p = 0.02$; Light*Day: $F_{(7,\ 46)} = 1.57$, $p > 0.05$. The results of Tukey's test, as q-values, are given in the text.

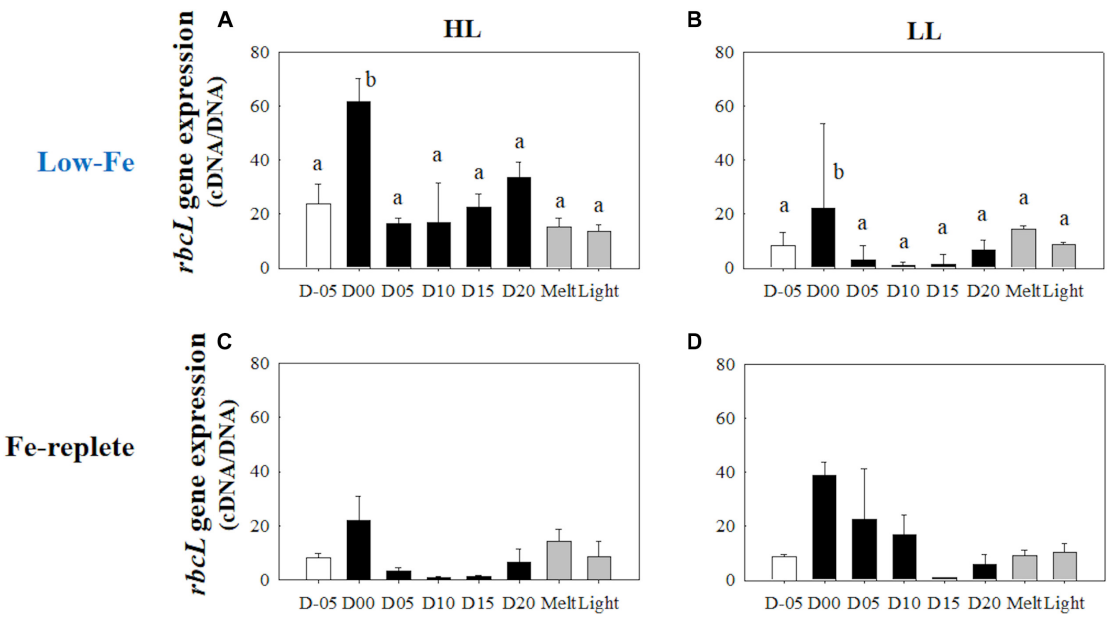

FIGURE 12 | Gene expression of the *rbcL* gene. Panels **(A,B)** show *rbcL* gene expression of the low-Fe ice tank runs in this study, whereas panels **(C,D)** show those of Fe-replete ice tank runs modified from Yoshida et al. (2020). Left **(A,C)** and right **(B,D)** panels indicate data from the HL and LL treatments, respectively. Open, closed, and shaded bars indicate values of pre-freeze seawater, ice, melted seawater samples, respectively. Letters above bars in a panel indicate significant differences in values between sampling days with one-way ANOVA with Tukey's test; there is no significant difference between values if a given letter is shown in the combination of letters of the counterparts. The D stands for "day," while Melt and Light indicate values after melting and light exposure experiments, respectively. Error bars show 1 standard deviation (n = 3). One-way ANOVA with Tukey's test, HL: $F_{(7,\ 23)} = 14.94$, $p < 0.001$; LL: $F_{(7,\ 23)} = 8.36$, $p < 0.001$. Two-way ANOVA test with Tukey's test, Light: $F_{(1,\ 45)} = 7.74$, $p < 0.001$; Day: $F_{(7,\ 45)} = 1.00$, $p > 0.05$; Light*Day: $F_{(7,\ 45)} = 0.79$, $p > 0.05$. The results of Tukey's test, as q-values, are given in the text.

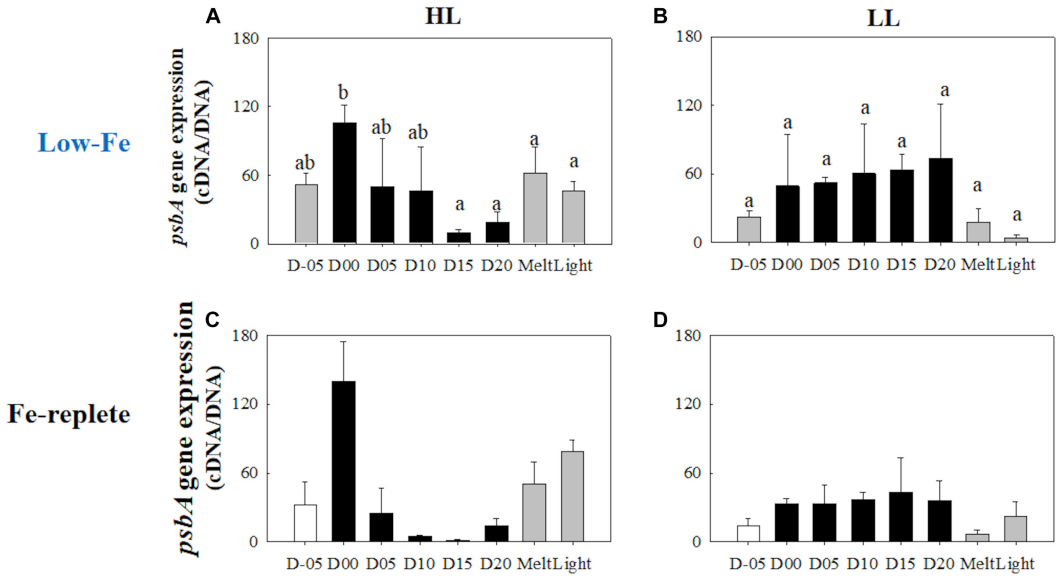

FIGURE 13 | Gene expression of the *psbA* gene. Panels **(A,B)** show *psbA* gene expression of the low-Fe ice tank runs in this study, whereas panels **(C,D)** show those of Fe-replete ice tank runs modified from Yoshida et al. (2020). Left **(A,C)** and right **(B,D)** panels indicate data from the HL and LL treatments, respectively. Open, closed, and shaded bars indicate values of pre-freeze seawater, ice, melted seawater samples, respectively. Letters above bars in a panel indicate significant differences in values between sampling days with one-way ANOVA with Tukey's test; there is no significant difference between values if a given letter is shown in the combination of letters of the counterparts. The D stands for "day," while Melt and Light indicate values after melting and light exposure experiments, respectively. Error bars show 1 standard deviation (n = 3). One-way ANOVA with Tukey's test, HL: $F_{(7,\ 23)}$ = 4.65, p = 0.005; LL: $F_{(7,\ 23)}$ = 2.33, $p >$ 0.05. Two-way ANOVA test with Tukey's test, Light: $F_{(1,\ 45)}$ = 3.82, $p >$ 0.05; Day: $F_{(7,\ 45)}$ = 2.58, p = 0.036; Light*Day: $F_{(7,\ 45)}$ = 3.16, p = 0.014. The results of Tukey's test, as q-values, are given in the text.

in α was due to increasing photosynthetic antennae size (i.e., increase in σ_{PSII}; "σ_{PSII} strategy," hereafter), but not increasing the number of photosynthetic units (n_{PSII} strategy). By conducting culture incubation experiments using representative Southern Ocean species, Strzepek et al. (2012, 2019), demonstrated that Southern Ocean phytoplankton in Fe-limited waters employed the σ_{PSII} strategy ($\sigma_{PSII} > 10$ nm^2 PSII^{-1}; Strzepek et al., 2019, similar in value to those of this study; **Figures 4A,B**). They proposed that the σ_{PSII} strategy is used to overcome Fe-light co-limitation in the Southern Ocean; this study is the first to demonstrate that ice algae in the Antarctic also appear to employ the same strategy. On the contrary, the Fe-replete ice tank experiments did not show any increase in both σ_{PSII} and α (**Figures 4C,D**, **6C,D**), indicating that the σ_{PSII} strategy could be a unique photophysiological response of polar diatoms to low-Fe and low-light conditions. Also, *F. cylindrus* had changed their low-light acclimation strategy; they increased n_{PSII} while being frozen in (n_{PSII} strategy; discussed above), whereas they enhanced σ_{PSII} over the duration of the frozen periods (σ_{PSII} strategy). This physiological switching in *F. cylindrus* could be significant for acclimation to ice environments.

Interestingly, NPQ_{NSV}' seemed to synchronize with DES during the frozen periods, whereas NPQ_{NSV}' and DES did not covary during the freezing event at day 00 (**Figures 5A,B**, **10A,B**), which was another evidence of the physiological switching. This response was feasible because DD and DT do not possess Fe, although there are some effects of Fe availability on the genetic translations of the pigments, such as operon regions (e.g., Laudenbach et al., 1988; Geider and LaRoche, 1994; Lommer et al., 2012; Georg et al., 2017). The DD-DT xanthophyll cycle was thus largely responsible for photoprotection in diatoms under the low-Fe condition, as well as high-Fe environments (Yan et al., 2019; Yoshida et al., 2020). The pool size of DD plus DT in the HL treatment was larger than that of the LL counterpart (**Figures 10A,B**), again suggesting more photoprotective capability under the HL condition. The significantly higher PPC/PSC ratio in the HL treatment was also supportive evidence of the large range of photoprotective capability (**Figures 11A,B**). NPQ'_{NSV} capability (maximum values of NPQ'_{NSV}) was, however, comparable between the HL and LL treatments (**Figures 5A,B**). This was possibly due to the effectiveness of the xanthophyll cycle rather than other factors, e.g., the cyclic electron flow via ferredoxin or flavodoxin (Prášil et al., 1996; Feikema et al., 2006; Cardol et al., 2011). The DD-DT xanthophyll cycle prevents further build-up of the transmembrane ΔpH because further electron sinks might not have been active. Indeed, Yoshida et al. (2020) reported that DES was not exclusively responsible for NPQ_{NSV}'; other electron pathways play supportive roles for photoprotection.

It is also of interest that both Schuback et al. (2015) and this study reported higher ETR_{max} values even under Fe starvation compared with Fe-replete conditions (Yoshida et al., 2020). The higher ETR_{max} values might also be due to charge recombination at PSII (i.e., reflux of electrons back to RCII after the excitation event; electron recoupling to RCII; Vass, 2011), leading to overestimation of electron transportation at

PSII (Schuback et al., 2016). The freezing stress could lead to high excitation pressure to the electron transport chain. Also, if the xanthophyll cycle was exclusively responsible for photoprotection, as discussed above, electron recoupling could be one of the possible pathways to address the enigmatic high ETR_{max} values under Fe starvation. Transcriptional activity of the *rbcL* gene was sharply downregulated in the ice and maintained at a low level (**Figures 12A,B**), suggesting that algal cells acclimated to their ice environment and optimized the balance between photochemical reactions and energy allocation to the dark reaction processes, such as carbon fixation by RuBisCO. It was of interest that *rbcL* gene expression in the HL treatment was significantly higher than the LL treatment (**Figures 12A,B**), suggesting that more RuBiSCO might be required as an electron sink with the higher excitation pressure in the HL treatment. The constant gene expression of the *psbA* gene in the LL treatment seems reasonable, as the constant freezing stress in the ice could have damaged the fragile D1 protein in PSII by over-reduction (**Figure 13A**). Downregulation in the transcriptional activity of the *psbA* gene in the HL treatment, however, was enigmatic because light stress was more evident at the higher light intensity. The relationship between the *psbA* gene and the transcription of the D1 protein is not directly inferred by the considerable post-transcriptional regulation (e.g., mRNA splicing and RNA editing; Kettunen et al., 1997). The significant upregulation of the *psbA* gene when frozen in (discussed above), associated with the sudden freezing stress, might thus provide excess mRNA to maintain synthesis of the D1 proteins.

Light Exposure After the Ice Melt Event

Even under low Fe availability, ice algae coped with light stress when they were released from sea ice. The high $ETR_{max,}$ values, which were higher than or similar to the Fe-replete values, also support the photosynthetic plasticity of *F. cylindrus* to the chronic low-Fe stress even after ice melt and light exposure (**Figure 7**; Yoshida et al., 2020). The σ_{PSII} strategy, which enlarges photosynthetic antenna size, was quite effective for photosynthetic acclimation to overcome low-Fe and low-light availability in sea ice (Strzepek et al., 2012, 2019). This low-Fe acclimation, at low temperatures, resulted in the similar growth rate to that of the Fe-replete ice tank runs. Light exposure significantly decreased F_v/F_m values due to the excess excitation pressure in the reaction centers of PSII, i.e., photoinhibition (**Figures 3A,B**; Melis, 1999). This photoinhibition was also evident even in the Fe-replete ice tank incubation experiments (Yoshida et al., 2020; **Figures 3C,D**). $NPQ_{NSV}{}'$ also responded to light exposure to dissipate excess energy (**Figures 5A,B**); however, photoprotective capability was not evident compared with Fe-replete condition (**Figures 5C,D**). The $NPQ_{NSV}{}'$ values in this low-Fe study were higher than those of the Fe-replete ice tank runs after the ice melt event (**Figure 5**). This upregulation of NPQ could be related to the σ_{PSII} strategy with the quite large photosynthetic antenna size. A larger antenna has a longer residence time of excitons within the PSII, which results in more energetic loss as NPQ (Raven, 1990; Wientjes et al., 2013; Strzepek et al., 2019). After the light exposure, the $NPQ_{NSV}{}'$ enhancement was less efficient (HL: 20.9% increase; LL: 57.8% increase) than in those of the Fe-replete conditions (HL: 98.5%; LL: 89.5% increase) reported in our previous ice-tank work (Yoshida et al., 2020; **Figure 5**). This indicates that the low Fe conditions suppressed NPQ ability. Moreover, the xanthophyll activity, shown as DES, was downregulated in the high light stress in the LL treatment, but not in the HL treatment (**Figures 10A,B**). This different response to light exposure reflects their different light history during the frozen period; lower photoprotective ability under lower light availability. In addition, the small change and lower DES after light provide a reasonable explanation of the lower $NPQ_{NSV}{}'$ enhancement. The xanthophyll pool and PPC/PSC ratio were, however, relatively stable, because pigment synthesis is slower than photoprotective processes (i.e., xanthophyll cycles and D1 protein repair) (Kuczynska et al., 2015).

The significant accumulation of chlide *a* after light exposure reflected the high level of absorbed energy that subsequently broke down intact chl *a*, possibly due to the presence of ROS (**Figures 9A,B**). The stable contribution of chlide *a* again implied that the production of chlide *a* was not due to ice melt events. Large concentrations of chlide *a*, however, have been observed at the surface of the Southern Ocean during ice retreat in spring (Bidigare et al., 1986; Wright et al., 2010). Exposure to high light after ice algae are released from ice is more likely the reason for the high chlide *a* contributions *in situ*. Interestingly, repair of damaged PSII, as indicated from gene expression of the *psbA* gene, was not activated after light exposure (**Figures 13A,B**). In addition, the slower repair of damaged PSII at low temperature (Kropuenske et al., 2009; van de Poll et al., 2011; Lacour et al., 2018) could exacerbate the photoinhibition. The diatom *F. cylindrus* displayed high photosynthetic flexibility and successfully acclimated to the low-Fe availability even after chronic Fe starvation in a simulated sea-ice environment. However, the chronic Fe starvation led to reduced photoprotective capability, which could affect the survival of ice algae when the cells are released to high-light pelagic waters. This might lead to changes in ice-edge bloom species and the extent of ice-edge blooms unless an ample amount of Fe is supplied to the cells during ice melt.

CONCLUSION

For the first time, we successfully incubated the polar diatom *F. cylindrus* under low Fe conditions in artificial sea ice using the ice tank. The artificial sea ice was similar to natural winter sea-ice characteristics including vertically elongated ice crystals and brine channels as well as brine pockets underneath a thin layer of fine granular frazil ice. Ice algae are capable of optimizing their photosynthesis for sea-ice environments during the freezing, ice melt and light exposure events even under chronic Fe starvation in sea ice. However, chronic Fe starvation led to reduced photoprotective capabilities. This may have detrimental consequences for ice algal production if the recent reduction in sea ice extent continues, although regional variabilities in the sea ice extent are evident around Antarctica (Stammerjohn and Maksym, 2017; Parkinson, 2019). Our study has revealed that Fe

availability modifies the photophysiological plasticity of ice algae. This also indicates that increased Fe availability in surface water would enhance phytoplankton growth and overwhelm ice algae after chronic Fe starvation in sea ice. A model simulation suggests a continued increase in Fe availability in the Southern Ocean (Boyd et al., 2015). Furthermore, glacial ice melt enhances the input of Fe to the surface water (Statham et al., 2008; Herraiz-Borreguero et al., 2016). Consequently, an Fe-related change in the production of ice algae and switching to phytoplankton dominance would change the diversity and trophic dynamics in the Southern Ocean (Constable et al., 2014). Our study emphasizes the importance of quantifying and modeling Fe availability in pack ice to predict changes in primary production and ecosystem functioning in low ice concentration zones around the Antarctic continent, including the Marginal Ice Zone (Boyd et al., 2016; Lannuzel et al., 2016b).

DATA AVAILABILITY STATEMENT

The data that support the findings of this study are available at: http://hdl.handle.net/2115/80350.

AUTHOR CONTRIBUTIONS

KY primarily wrote the manuscript, collected and interpreted the data. AM and KS supervised KY and conceptualized the study. KY, AS, and AM designed the ice tank experiments. KY, AS, KK, and AM developed low-Fe ice tank techniques. KY, MC, and PH conducted the ice structure measurement. MC and PH interpreted results of the ice structure measurement and wrote the manuscript. AS, MC, PH, AM, and KS critically revised the manuscript. All authors contributed to the article and approved the submitted version.

FUNDING

This study was supported by the Australian Antarctic Programme (AAS4319). The *Fragilariopsis cylindrus* collection was supported under the Australian Research Council's Special Research Initiative for Antarctic Gateway Partnership (Project ID SR140300001). The structural analysis was supported by AAS4506. This study was also partly supported by the JSPS Grants-in-Aid for Scientific Research (JP18H03352 and JP17H00775).

SUPPLEMENTARY MATERIAL

The Supplementary Material for this article can be found online at: https://www.frontiersin.org/articles/10.3389/fmars.2021.632087/full#supplementary-material

REFERENCES

Arrigo, K. R. (2017). "Sea ice as a habitat for primary producers," in *Sea Ice*, 3rd Edn, ed. D. N. Thomas (West Sussex: Wiley Blackwell), 352–369.

Arrigo, K. R., Worthen, D. L., Lizotte, M. P., Dixon, P., and Dieckmann, G. S. (1997). Primary production in antarctic sea ice. *Science* 276, 394–397. doi: 10.1126/science.276.5311.394

Behrenfeld, M. J., and Milligan, A. J. (2013). Photophysiological expressions of iron stress in phytoplankton. *Ann. Rev. Mar. Sci.* 5, 217–246. doi: 10.1146/annurev-marine-121211-172356

Bidigare, R. R., Frank, T. J., Zastrow, C., and Brooks, J. M. (1986). The distribution of algal chlorophylls and their degradation products in the Southern Ocean. *Deep Sea Res. A Oceanogr. Res. Pap.* 33, 923–937. doi: 10.1016/0198-0149(86)90007-5

Boyd, P. W., Dillingham, P. W., Mcgraw, C. M., Armstrong, E. A., Cornwall, C. E., Feng, Y. Y., et al. (2016). Physiological responses of a Southern Ocean diatom to complex future ocean conditions. *Nat. Clim. Chang.* 6, 207–213. doi: 10.1038/nclimate2811

Boyd, P. W., Lennartz, S. T., Glover, D. M., and Doney, S. C. (2015). Biological ramifications of climate-change-mediated oceanic multi-stressors. *Nat. Clim. Chang.* 5, 71–79. doi: 10.1038/nclimate2441

Breitbarth, E., Gelting, J., Walve, J., Hoffmann, L. J., Turner, D. R., Hassellov, M., et al. (2009). Dissolved iron (II) in the Baltic Sea surface water and implications for cyanobacterial bloom development. *Biogeosciences* 6, 2397–2420.

Bricaud, A., Babin, M., Morel, A., and Claustre, H. (1995). Variability in the chlorophyll-specific absorption coefficients of natural phytoplankton: analysis and parameterization. *J. Geophys. Res.* 100, 13321–13332. doi: 10.1029/95JC00463

Britton, D., Mundy, C. N., McGraw, C. M., Revill, A. T., Hurd, C. L., and Norkko, J. (2019). Responses of seaweeds that use CO_2 as their sole inorganic carbon source to ocean acidification: differential effects of fluctuating pH but little benefit of CO_2 enrichment. *ICES J. Mar. Sci.* 76, 1860–1870. doi: 10.1093/icesjms/fsz070

Cardol, P., Forti, G., and Finazzi, G. (2011). Regulation of electron transport in microalgae. *Biochim. Biophys. Acta Bioenerg.* 1807, 912–918. doi: 10.1016/j.bbabio.2010.12.004

Constable, A. J., Melbourne-Thomas, J., Corney, S. P., Arrigo, K. R., Barbraud, C., Barnes, D. K. A., et al. (2014). Climate change and Southern Ocean ecosystems I: how changes in physical habitats directly affect marine biota. *Glob. Chang. Biol.* 20, 3004–3025. doi: 10.1111/gcb.12623

Cutter, G. A., Casciotti, K., Croot, P., Geibert, W., Heimbürger, L. E., Lohan, M. C., et al. (2017). *Sampling and Sample-Handling Protocols for Geotraces Cruises, Version 3.0*. Toulouse: GEOTRACES International Project Office.

de Jong, J., Schoemann, V., Maricq, N., Mattielli, N., Langhorne, P., Haskell, T., et al. (2013). Iron in land-fast sea ice of McMurdo Sound derived from sediment resuspension and wind-blown dust attributes to primary productivity in the Ross Sea Antarctica. *Mar. Chem.* 157, 24–40. doi: 10.1016/j.marchem.2013.07.001

de Jong, J. T. M., Stammerjohn, S. E., Ackley, S. F., Tison, J.-L., Mattielli, N., and Schoemann, V. (2015). Sources and fluxes of dissolved iron in the Bellingshausen Sea (West Antarctica): the importance of sea ice, icebergs and the continental margin. *Mar. Chem.* 177, 518–535. doi: 10.1016/j.marchem.2015.08.004

Devos, N., Ingouff, M., Loppes, R., and Matagne, R. F. (1998). Rubisco adaptation to low temperatures: a comparative study in psychrophilic and mesophilic unicellular algae. *J. Phycol.* 34, 655–660. doi: 10.1046/j.1529-8817.1998.340655.x

Endo, H., Sugie, K., Yoshimura, T., and Suzuki, K. (2015). Effects of CO_2 and iron availability on rbc gene expression in Bering Sea diatoms. *Biogeosciences* 12, 2247–2259. doi: 10.5194/bg-12-2247-2015

Endo, H., Yoshimura, T., Kataoka, T., and Suzuki, K. (2013). Effects of CO_2 and iron availability on phytoplankton and eubacterial community compositions in the northwest subarctic Pacific. *J. Exp. Mar. Bio. Ecol.* 439, 160–175. doi: 10.1016/j.jembe.2012.11.003

Falkowski, P. G., and Owens, T. G. (1980). Light-shade adaptation: two strategies in marine phytoplankton. *Plant Physiol.* 66, 592–595. doi: 10.1104/pp.66.4.592

Farid, T. H., Schulz, K. G., and Rose, A. L. (2018). Measuring total dissolved Fe concentrations in phytoplankton cultures in the presence of synthetic and organic ligands using a modified ferrozine method. *Mar. Chem.* 203, 22–27. doi: 10.1016/j.marchem.2018.04.003

Feikema, W. O., Marosvölgyi, M. A., Lavaud, J., and van Gorkom, H. J. (2006). Cyclic electron transfer in photosystem II in the marine diatom *Phaeodactylum tricornutum*. *Biochim. Biophys. Acta* 1757, 829–834. doi: 10.1016/j.bbabio.2006.06.003

Fernández-Méndez, M., Katlein, C., Rabe, B., Nicolaus, M., Peeken, I., Bakker, K., et al. (2015). Photosynthetic production in the central Arctic Ocean during the record sea-ice minimum in 2012. *Biogeosciences* 12, 3525–3549. doi: 10.5194/bg-12-3525-2015

Geider, R. J., and LaRoche, J. (1994). The role of iron in phytoplankton photosynthesis, and the potential for iron-limitation of primary productivity in the sea. *Photosynth. Res.* 39, 275–301. doi: 10.1007/BF00014588

Genovese, C., Grotti, M., Pittaluga, J., Ardini, F., Janssens, J., Wuttig, K., et al. (2018). Influence of organic complexation on dissolved iron distribution in East Antarctic pack ice. *Mar. Chem.* 203, 28–37. doi: 10.1016/j.marchem.2018.04.005

Georg, J., Kostova, G., Vuorijoki, L., Schön, V., Kadowaki, T., Huokko, T., et al. (2017). Acclimation of oxygenic photosynthesis to iron starvation is controlled by the sRNA IsaR1. *Curr. Biol* 27, 1425–1436.e7. doi: 10.1016/j.cub.2017.04.010

Golden, K. M., Ackley, S. F., and Lytle, V. I. (1998). The percolation phase transition in sea ice. *Science* 282, 2238–2241. doi: 10.1126/science.282.5397.2238

Govindjee, Kern, J. F., Messinger, J., and Whitmarsh, J. (2010). "Photosystem II," in *eLS*. doi: 10.1002/9780470015902.a0000669.pub2

Greene, R. M., Geider, R. J., Kolber, Z., and Falkowski, P. G. (1992). Iron-induced changes in light harvesting and photochemical energy conversion processes in eukaryotic marine algae. *Plant Physiol.* 100, 565–575. doi: 10.1104/pp.100.2.565

Herraiz-Borreguero, L., Lannuzel, D., Treverrow, A., van der Merwe, P., and Pedro, J. (2016). Contribution of marine ice iron to the fertilization of Prydz Bay, East Antarctica. *J. Geophys. Res. Oceans* 121:8. doi: 10.1002/2016JC011687

Huot, Y., and Babin, M. (2011). "Overview of fluorescence protocols: theory, basic concepts, and practice," in *Chlorophyll a Fluorescence in Aquatic Sciences: Methods and Applications*, eds D. J. Suggett, O. Prášil, and M. A. Borowitzka (Amsterdam: Springer), 31–74.

Janssens, J., Meiners, K. M., Tison, J.-L., Dieckmann, G., Delille, B., and Lannuzel, D. (2016). Incorporation of iron and organic matter into young Antarctic sea ice during its initial growth stages. *Elem. Sci. Anthr.* 4:000123. doi: 10.12952/journal.elementa.000123

Kameyama, S., Otomaru, M., McMinn, A., and Suzuki, K. (2020). Ice melting can change DMSP production and photosynthetic activity of the haptophyte *Phaeocystis antarctica*. *J. Phycol.* 56, 761–774. doi: 10.1111/jpy.12985

Katayama, T., Makabe, R., Sampei, M., Hattori, H., Sasaki, H., and Taguch, S. (2017). Photoprotection and recovery of photosystem II in the Southern Ocean phytoplankton. *Polar Sci.* 12, 5–11. doi: 10.1016/j.polar.2016.12.003

Katayama, T., and Taguchi, S. (2013). Photoprotective responses of ice algal community in Saroma-Ko Lagoon, Hokkaido, Japan. *Polar Biol.* 36, 1431–1439.

Kennedy, F., Martin, A., Bowman, J. P., Wilson, R., and McMinn, A. (2019). Dark metabolism: a molecular insight into how the Antarctic sea-ice diatom *Fragilariopsis cylindrus* survives long-term darkness. *New Phytol.* 223, 675–691. doi: 10.1111/nph.15843

Kennedy, F., McMinn, A., and Martin, A. (2012). Effect of temperature on the photosynthetic efficiency and morphotype of *Phaeocystis antarctica*. *J. Exp. Mar. Bio. Ecol.* 429, 7–14. doi: 10.1016/j.jembe.2012.06.016

Kettunen, R., Pursiheimo, S., Rintamaki, E., van Wijk, K., and Aro, E. (1997). Transcriptional and translational adjustments of *psbA* gene expression in mature chloroplasts during photoinhibition and subsequent repair of photosystem II. *Eur. J. Biochem.* 247, 441–448.

Kolber, Z. S., Barber, R. T., Coale, K. H., Fitzwater, S. E., Greene, R. M., Johnson, K. S., et al. (1994). Iron limitatiton of phytoplankton photosynthesis in the equatorial Pacific Ocean. *Nature* 371, 145–149. doi: 10.1038/383508a0

Kolber, Z. S., Prášil, O., and Falkowski, P. G. (1998). Measurements of variable chlorophyll fluorescence using fast repetition rate techniques: defining methodology and experimental protocols. *Biochim. Biophys. Acta* 1367, 88–106. doi: 10.1016/S0005-2728(98)00135-2

Krembs, C., Eicken, H., Junge, K., and Deming, J. W. (2002). High concentrations of exopolymeric substances in Arctic winter sea ice: implications for the polar ocean carbon cycle and cryoprotection of diatoms. *Deep Sea Res. I* 49, 2163–2181. doi: 10.1016/S0967-0637(02)00122-X

Kropuenske, L. R., Mills, M. M., van Dijken, G. L., Bailey, S., Robinson, D. H., Welschmeyer, N. A., et al. (2009). Photophysiology in two major southern ocean phytoplankton taxa: photoprotection in *Phaeocystis antarctica* and *Fragilariopsis cylindrus*. *Limnol. Ocean.* 54, 1176–1196. doi: 10.1093/icb/icq021

Kuczynska, P., Jemiola-Rzeminska, M., and Strzalka, K. (2015). Photosynthetic pigments in diatoms. *Mar. Drugs* 13, 5847–5881. doi: 10.3390/md13095847

Lacour, T., Larivière, J., Ferland, J., Bruyant, F., Lavaud, J., and Babin, M. (2018). The role of sustained photoprotective non-photochemical quenching in low temperature and high light acclimation in the bloom-forming Arctic diatom *Thalassiosira gravida*. *Front. Mar. Sci.* 5:354. doi: 10.3389/fmars.2018.00354

Langway, C. C. (1958). *Ice Fabrics and the Universal Stage*, Vol. 62. Pentagon, VA.: Department of the Army.

Lannuzel, D., Chever, F., van der Merwe, P. C., Janssens, J., Roukaerts, A., Cavagna, A. J., et al. (2016a). Iron biogeochemistry in Antarctic pack ice during SIPEX-2. *Deep Sea Res. II* 131, 111–122. doi: 10.1016/j.dsr2.2014.12.003

Lannuzel, D., Grotti, M., Abelmoschi, M. L., and van der Merwe, P. (2015). Organic ligands control the concentrations of dissolved iron in Antarctic sea ice. *Mar. Chem.* 174, 120–130. doi: 10.1016/j.marchem.2015.05.005

Lannuzel, D., Schoemann, V., de Jong, J., Chou, L., Delille, B., Becquevort, S., et al. (2008). Iron study during a time series in the western Weddell pack ice. *Mar. Chem.* 108, 85–95. doi: 10.1016/j.marchem.2007.10.006

Lannuzel, D., Schoemann, V., de Jong, J., Tison, J.-L., and Chou, L. (2007). Distribution and biogeochemical behaviour of iron in the East Antarctic sea ice. *Mar. Chem.* 106, 18–32. doi: 10.1016/j.marchem.2006.06.010

Lannuzel, D., Schoemann, V., Dumont, I., de Jong, J., Tison, J.-L., Delille, B., et al. (2013). Effect of melting Antarctic sea ice on the fate of microbial communities studied in microcosms. *Polar Biol.* 36, 1483–1497. doi: 10.1007/s00300-013-1368-7

Lannuzel, D., van der Merwe, P. C., Townsend, A. T., and Bowie, A. R. (2014). Size fractionation of iron, manganese and aluminium in Antarctic fast ice reveals a lithogenic origin and low iron solubility. *Mar. Chem.* 161, 47–56. doi: 10.1016/j.marchem.2014.02.006

Lannuzel, D., Vancoppenolle, M., van der Merwe, P., de Jong, J., Meiners, K. M., Grotti, M., et al. (2016b). Iron in sea ice: review and new insights. *Elem. Sci. Anthr.* 4:000130. doi: 10.12952/journal.elementa.000130

Laudenbach, D. E., Reith, M. E., and Straus, N. A. (1988). Isolation, sequence analysis, and transcriptional studies of the flavodoxin gene from *Anacystis nidulans* R2. *J. Bacteriol.* 170, 258–265. doi: 10.1128/jb.170.1.258-265.1988

Legendre, L., Ackley, S., Dieckmann, G., Gulliksen, B., Horner, R., Hoshiai, T., et al. (1992). Ecology of sea ice biota 2. Global significance. *Polar Biol.* 12, 429–444. doi: 10.1007/BF00243114

Lommer, M., Specht, M., Roy, A. S., Kraemer, L., Andreson, R., Gutowska, M. A., et al. (2012). Genome and low-iron response of an oceanic diatom adapted to chronic iron limitation. *Genome Biol.* 13:R66. doi: 10.1186/gb-2012-13-7-r66

Lyon, B. R., and Mock, T. (2014). Polar microalgae: new approaches towards understanding adaptation to an extreme and changing environment. *Biology* 3, 56–80. doi: 10.3390/biology3010056

Maldonado, M. T., Boyd, P. W., Harrison, P. J., and Price, N. M. (1999). Co-limitation of phytoplankton growth by light and Fe during winter in the NE subarctic Pacific Ocean. *Deep. Res. II Top. Stud. Oceanogr.* 46, 2475–2485. doi: 10.1016/S0967-0645(99)00072-7

Matson, P. G., Washburn, L., Martz, T. R., and Hofmann, G. E. (2014). Abiotic versus biotic drivers of ocean pH variation under fast sea ice in McMurdo Sound, Antarctica. *PLoS One* 9:e107239. doi: 10.1371/journal.pone.0107239

McKew, B. A., Davey, P., Finch, S. J., Hopkins, J., Lefebvre, S. C., Metodiev, M. V., et al. (2013). The trade-off between the light-harvesting and photoprotective functions of fucoxanthin-chlorophyll proteins dominates light acclimation in *Emiliania huxleyi* (clone CCMP 1516). *New Phytol.* 200, 74–85. doi: 10.1111/nph.12373

McMinn, A., Muller, M. N., Martin, A., and Ryan, K. G. (2014). The response of Antarctic sea ice algae to changes in pH and CO_2. *PLoS One* 9:e86984. doi: 10.1371/journal.pone.0044459

McMinn, A., Pankowski, A., Ashworth, C., Bhagooli, R., Ralph, P., and Ryan, K. (2010). In situ net primary productivity and photosynthesis of Antarctic sea ice algal, phytoplankton and benthic algal communities. *Mar. Biol.* 157, 1345–1356. doi: 10.1007/s00227-010-1414-8

Meiners, K. M., Vancoppenolle, M., Carnat, G., Castellani, G., Delille, B., Delille, B., et al. (2018). Chlorophyll-*a* in Antarctic landfast sea ice: a first synthesis of historical ice core data. *J. Geophys. Res. Oceans* 123, 8444–8459. doi: 10.1029/2018JC014245

Meiners, K. M., Vancoppenolle, M., Thanassekos, S., Dieckmann, G. S., Thomas, D. N., Tison, J.-L., et al. (2012). Chlorophyll *a* in Antarctic sea ice from historical ice core data. *Geophys. Res. Lett*. 39:21. doi: 10.1029/2012GL053478

Melis, A. (1999). Photosystem-II damage and repair cycle in chloroplasts: what modulates the rate of photodamage in vivo? *Trends Plant Sci.* 4, 130–135. doi: 10.1016/S1360-1385(99)01387-4

Millero, F., Woosley, R., DiTrolio, B., and Waters, J. (2009). Effect of ocean acidification on the speciation of metals in seawater. *Oceanography* 22, 72–85. doi: 10.5670/oceanog.2009.98

Millero, F. J., Sotolongo, S., and Izaguirre, M. (1987). The oxidation kinetics of Fe (II) in seawater. *Geochim. Cosmochim. Acta* 51, 793–801.

Mock, T., Otillar, R. P., Strauss, J., McMullan, M., Paajanen, P., Schmutz, J., et al. (2017). Evolutionary genomics of the cold-adapted diatom *Fragilariopsis cylindrus*. *Nature* 541, 536–540. doi: 10.1038/nature20803

Moore, C. M., Seeyave, S., Hickman, A. E., Allen, J. T., Lucas, M. I., Planquette, H., et al. (2007). Iron–light interactions during the CROZet natural iron bloom and EXport experiment (CROZEX) I: phytoplankton growth and photophysiology. *Deep. Res. II* 54, 2045–2065. doi: 10.1016/j.dsr2.2007.06.011

Morel, A., and Bricaud, A. (1981). Theoretical results concerning light absorption in a discrete medium, and application to specific absorption of phytoplankton. *Deep. Sea Res. A* 28, 1375–1393. doi: 10.1016/0198-0149(81)90039-X

Oxborough, K., and Baker, N. R. (1997). Resolving chlorophyll *a* fluorescence images of photosynthetic efficiency into photochemical and non-photochemical components – calculation of *qP* and *Fv'/Fm'* without measuring *Fo'*. *Photosynth. Res.* 54, 135–142. doi: 10.1023/A:1005936823310

Pankowski, A., and McMinn, A. (2008). Ferredoxin and flavodoxin in eastern Antarctica pack ice. *Polar Biol.* 31, 1153–1165. doi: 10.1007/s00300-008-0451-y

Pankowski, A., and McMinn, A. (2009). Iron availability regulates growth, photosynthesis, and production of ferredoxin and flavodoxin in Antarctic sea ice diatoms. *Aquat. Biol.* 4, 273–288. doi: 10.3354/ab00116

Parkinson, C. L. (2019). A 40-y record reveals gradual Antarctic sea ice increases followed by decreases at rates far exceeding the rates seen in the Arctic. *Proc. Natl. Acad. Sci. U.S.A.* 116, 14414–14423. doi: 10.1073/pnas.1906556116

Parsons, T. R., Maita, Y., and Lalli, C. M. (1984). *A Manual of Chemical and Biological Methods for Seawater Analysis*. Oxford: Pergamon Press.

Petrich, C., and Eicken, H. (2017). "Overview of sea ice growth and properties," in *Sea Ice*, 3rd Edn, ed. D. N. Thomas (West Sussex: Wiley Blackwell), 1–41.

Petrou, K., Trimborn, S., Rost, B., Ralph, P. J., and Hassler, C. S. (2014). The impact of iron limitation on the physiology of the Antarctic diatom *Chaetoceros simplex*. *Mar. Biol.* 161, 925–937. doi: 10.1007/s00227-014-2392-z

Platt, T., Gallegos, C. L., and Harrison, W. G. (1980). Photoinibition of photosynthesis in natural assemblages of marine phytoplankton. *J. Mar. Res.* 38, 687–701.

Prášil, O., Kolber, Z., Berry, J. A., and Falkowski, P. G. (1996). Cyclic electron flow around Photosystem II *in vivo*. *Photosynth. Res.* 48, 395–410.

Price, N. M., Harrison, G. I., Hering, J. G., Hudson, R. J., Nirel, P. M. V., Palenik, B., et al. (1989). Preparation and chemistry of the artificial algal culture medium Aquil. *Biol. Oceanogr.* 6, 443–461. doi: 10.1080/01965581.1988.10749544

Raven, J. A. (1990). Predictions of Mn and Fe use efficiencies of phototrophic growth as a function of light availability for growth and of C assimilation pathway. *New Phytol.* 116, 1–18. doi: 10.1111/j.1469-8137.1990.tb00505.x

Rintala, J. M., Piiparinen, J., Blomster, J., Majaneva, M., Müller, S., Uusikivi, J., et al. (2014). Fast direct melting of brackish sea-ice samples results in biologically more accurate results than slow buffered melting. *Polar Biol.* 37, 1811–1822. doi: 10.1007/s00300-014-1563-1

Roncel, M., González-rodríguez, A. A., Naranjo, B., Bernal-bayard, P., Lindahl, A. M., Hervás, M., et al. (2016). Iron deficiency induces a partial inhibition of the photosynthetic electron transport and a high sensitivity to light in the diatom *Phaeodactylum tricornutum*. *Front. Plant Sci.* 7:1050. doi: 10.3389/fpls.2016.01050

Satoh, H., Yamaguchi, Y., Watanabe, K., Tanimura, A., Fukuchi, M., and Aruga, Y. (1989). "Photosynthetic nature of ice algae and their contribution to the primary production in Lagoon Saroma Ko, Hokkaido, Japan," in *Proceedings of National Institute of Polar Research Symposium on Polar Biology*, Vol. 2. (Tokyo: Tokyo National Institute of Polar Research), 1–8.

Schuback, N., Flecken, M., Maldonado, M. T., and Tortell, P. D. (2016). Diurnal variation in the coupling of photosynthetic electron transport and carbon fixation in iron-limited phytoplankton in the NE subarctic Pacific. *Biogeosciences* 13, 1019–1035. doi: 10.5194/bg-13-1019-2016

Schuback, N., Schallenberg, C., Duckham, C., Maldonado, M. T., and Tortell, P. D. (2015). Interacting effects of light and iron availability on the coupling of photosynthetic electron transport and CO_2-assimilation in marine phytoplankton. *PLoS One* 10:e0133235. doi: 10.1371/journal.pone.0133235

Shi, D., Xu, Y., Hopkinson, B. M., and Morel, F. M. M. (2010). Effect of ocean acidification on iron availability to marine phytoplankton. *Science* 327, 676–679. doi: 10.1126/science.1183517

Smith, W. O., and Nelson, D. M. (1986). Importance of ice edge phytoplankton production in the Southern Ocean. *Bioscience* 36, 251–257. doi: 10.2307/1310215

Stammerjohn, S., and Maksym, T. (2017). "Gaining (and losing) Antarctic sea ice: variability, trends and mechanisms," in *Sea Ice*, 3rd Edn, ed. D. N. Thomas (West Sussex: Wiley Blackwell), 261–289.

Statham, P. J., Skidmore, M., and Tranter, M. (2008). Inputs of glacially derived dissolved and colloidal iron to the coastal ocean and implications for primary productivity. *Glob. Biogeochem. Cycles* 22:GB3013. doi: 10.1029/2007GB003106

Steiner, N., Deal, C., Lannuzel, D., Lavoie, D., Massonnet, F., Miller, L. A., et al. (2016). What sea-ice biogeochemical modellers need from observers. *Elem. Sci. Anthr.* 4:000084. doi: 10.12952/journal.elementa.000084

Stookey, L. L. (1970). Ferrozine – a new spectrophotometric reagent for iron. *Can. J. Chem.* 62, 721–724. doi: 10.1021/ac60289a016

Strzepek, R. F., Boyd, P. W., and Sunda, W. G. (2019). Photosynthetic adaptation to low iron, light, and temperature in Southern Ocean phytoplankton. *Proc. Natl. Acad. Sci. U.S.A.* 116, 4388–4393. doi: 10.1073/pnas.1810886116

Strzepek, R. F., Hunter, K. A., Frew, R. D., Harrison, P. J., and Boyd, P. W. (2012). Iron-light interactions differ in Southern Ocean phytoplankton. *Limnol. Oceanogr.* 57, 1182–1200. doi: 10.4319/lo.2012.57.4.1182

Suggett, D. J., Prášil, O., and Borowitzka, M. A. (2011). *Chlorophyll a Fluorescence in Aquatic Sciences: Methods and Applications*. New York, NY: Springer.

Sunda, W., and Huntsman, S. (2003). Effect of pH, light, and temperature on Fe-EDTA chelation and Fe hydrolysis in seawater. *Mar. Chem.* 84, 35–47. doi: 10.1016/S0304-4203(03)00101-4

Sunda, W. G., and Huntsman, S. A. (1995). Iron uptake and growth limitation in oceanic and coastal phytoplankton. *Mar. Chem.* 50, 189–206.

Sunda, W. G., and Huntsman, S. A. (1997). Interrelated influence of iron, light and cell size on marine phytoplankton growth. *Nature* 390, 389–391. doi: 10.1038/37093

Suzuki, K., Kamimura, A., and Hooker, S. B. (2015). Rapid and highly sensitive analysis of chlorophylls and carotenoids from marine phytoplankton using ultra-high performance liquid chromatography (UHPLC) with the first derivative spectrum chromatogram (FDSC) technique. *Mar. Chem.* 176, 96–109. doi: 10.1016/j.marchem.2015.07.010

Suzuki, K., Liu, H., Saino, T., Obata, H., Takano, M., Okamura, K., et al. (2002). East-west gradients in the photosynthetic potential of phytoplankton and iron concentration in the subarctic Pacific Ocean during early summer. *Limnol. Oceanogr.* 47, 1581–1594. doi: 10.4319/lo.2002.47.6.1581

Syvertsen, E. E. (1991). Ice algae in the Barents Sea: types of assemblages, origin, fate and role in the ice−edge phytoplankton bloom. *Polar Res.* 10, 277–288. doi: 10.1111/j.1751-8369.1991.tb00653.x

Tagliabue, A., Mtshali, T., Aumont, O., Bowie, A. R., Klunder, M. B., Roychoudhury, A. N., et al. (2012). A global compilation of dissolved iron measurements: focus on distributions and processes in the Southern Ocean. *Biogeosciences* 9, 2333–2349. doi: 10.5194/bg-9-2333-2012

Tedesco, L., Vichi, M., and Scoccimarro, E. (2019). Sea-ice algal phenology in a warmer Arctic. *Sci. Adv.* 5:eaav4830. doi: 10.1126/sciadv.aav4830

Thomas, D. N., and Dieckmann, G. S. (2002). Antarctic sea ice-a habitat for extremophiles. *Science* 295, 641–644. doi: 10.1126/science.1063391

Twining, B. S., and Baines, S. B. (2013). The trace metal composition of marine phytoplankton. *Ann. Rev. Mar. Sci.* 5, 191–215. doi: 10.1146/annurev-marine-121211-172322

van de Poll, W. H., Lagunas, M., De Vries, T., Visser, R. J. W., and Buma, A. G. J. (2011). Non-photochemical quenching of chlorophyll fluorescence and xanthophyll cycle responses after excess PAR and UVR in *Chaetoceros brevis*, *Phaeocystis antarctica* and coastal Antarctic phytoplankton. *Mar. Ecol. Prog. Ser.* 426, 119–131. doi: 10.3354/meps09000

van der Merwe, P., Lannuzel, D., Bowie, A. R., Nichols, C. M., and Meiners, K. M. (2011). Iron fractionation in pack and fast ice in East Antarctica: temporal decoupling between the release of dissolved and particulate iron during spring melt. *Deep Sea Res. II* 58, 1222–1236. doi: 10.1016/j.dsr2.2010.10.036

van Leeuwe, M. A., Tedesco, L., Arrigo, K. R., Assmy, P., Campbell, K., Meiners, K. M., et al. (2018). Microalgal community structure and primary production in Arctic and Antarctic sea ice: a synthesis. *Elem. Sci. Anth.* 6:4. doi: 10.1525/elementa.267

van Oijen, T., van Leeuwe, M. A., Gieskes, W. W. C., and de Baar, H. J. W. (2004). Effects of iron limitation on photosynthesis and carbohydrate metabolism in the Antarctic diatom *Chaetoceros brevis* (Bacillariophyceae). *Eur. J. Phycol.* 39, 161–171. doi: 10.1080/0967026042000202127

Vancoppenolle, M., Bopp, L., Madec, G., Dunne, J., Ilyina, T., Halloran, P. R., et al. (2013). Future Arctic Ocean primary productivity from CMIP5 simulations: uncertain outcome, but consistent mechanisms. *Glob. Biogeochem. Cycles* 27, 605–619. doi: 10.1002/gbc.20055

Vass, I. (2011). Role of charge recombination processes in photodamage and photoprotection of the photosystem II complex. *Physiol. Plant.* 142, 6–16. doi: 10.1111/j.1399-3054.2011.01454.x

Wientjes, E., van Amerongen, H., and Croce, R. (2013). Quantum yield of charge separation in photosystem II: functional effect of changes in the antenna size upon light acclimation. *J. Phys. Chem. B* 117, 11200–11208. doi: 10.1021/jp401663w

Wongpan, P., Meiners, K. M., Langhorne, P. J., Heil, P., Smith, I. J., Leonard, G. H., et al. (2018). Estimation of Antarctic land-fast sea ice algal biomass and snow thickness from under-ice radiance spectra in two contrasting areas. *J. Geophys. Res. Ocean.* 123, 1907–1923. doi: 10.1002/2017JC013711

Wood, A. M., Everroad, R. C., and Wingard, L. M. (2005). "Measuring growth rates in microalgal culture," in *Algal Culturing Techniques*, ed. R. A. Andersen (Amsterdam: Elsevier), 269–285.

Wright, S. W., van den Enden, R. L., Pearce, I., Davidson, A. T., Scott, F. J., and Westwood, K. J. (2010). Phytoplankton community structure and stocks in the Southern Ocean (30-80°E) determined by CHEMTAX analysis of HPLC pigment signatures. *Deep. Res. II* 57, 758–778. doi: 10.1016/j.dsr2.2009.06.015

Yan, D., Endo, H., and Suzuki, K. (2019). Increased temperature benefits growth and photosynthetic performance of the sea ice diatom *Nitzschia* cf. *neglecta* (Bacillariophyceae) isolated from saroma lagoon, Hokkaido, Japan. *J. Phycol.* 55, 700–713. doi: 10.1111/jpy.12846

Yoshida, K., Endo, H., Lawrenz, E., Isada, T., Hooker, S. B., Prášil, O., et al. (2018). Community composition and photophysiology of phytoplankton assemblages in coastal Oyashio waters of the western North Pacific during early spring. *Estur. Coast. Shelf Sci.* 212, 80–94. doi: 10.1016/j.ecss.2018.06.018

Yoshida, K., Seger, A., Kennedy, F., McMinn, A., and Suzuki, K. (2020). Freezing, melting and light stress on the photophysiology of ice algae: *ex situ* incubation of the ice algal diatom *Fragilariopsis cylindrus* (Bacillariophyceae) using an ice tank. *J. Phycol.* 56, 1323–1338. doi: 10.1111/jpy.13036

Young, J. N., Goldman, J. A. L., Kranz, S. A., Tortell, P. D., and Morel, F. M. M. (2015). Slow carboxylation of Rubisco constrains the rate of carbon fixation during Antarctic phytoplankton blooms. *New Phytol.* 205, 172–181. doi: 10.1111/nph.13021

Conflict of Interest: The authors declare that the research was conducted in the absence of any commercial or financial relationships that could be construed as a potential conflict of interest.